Roles of transcription factor AP-2β in sleep regulation in mice
(マウスの睡眠制御における転写因子 AP-2β の機能の解析)

令和 4 年度

中　井　彩　加
筑波大学大学院人間総合科学学術院人間総合科学研究群
ニューロサイエンス学位プログラム

Table of contents

Abstract

The molecular mechanism of sleep remains to be elucidated. This study focused on the transcription factor AP-2β (TFAP2B). Sleep abnormalities such as short sleep and sleep-walking have been self-reported in human families that carry mutations in TFAP2B. Moreover, the mutation or knockdown of genes encoding AP-2 transcription factors in invertebrate animals result in reduced sleep. Thus, AP-2 transcription factors might have a conserved role in sleep regulation across the animal phyla. However, direct evidence supporting the involvement of TFAP2B in mammalian sleep was lacking. Herein, I demonstrate that different mutations in *Tfap2b* lead to diverse effects on sleep architecture, including the reduction or fragmentation of non-rapid eye movement sleep (Nakai *et al.*, *Genetics* 2020). I analyzed two *Tfap2b* mutant mouse strains mimicking the mutations in human kindreds that self-reported sleep abnormalities. Moreover, I analyzed the sleep/wake cycle of heterozygous *Tfap2b* knockout (KO) mice and nervous system-specific homozygous *Tfap2b* KO mice and found that these mice also exhibit reduced non-REM sleep. In conclusion, different mutations in *Tfap2b* can lead to diverse effects on sleep architecture and that TFAP2B is required for the development of normal sleep patterns in mice.

Introduction

Search for natural short sleep-related genes

Sleep is a physiological state widely observed in animals. Not only mammals but also birds, reptiles, fish, and invertebrates exhibit sleep. Many animals exhibit rhythms that consist of active and inactive periods. There are five definitions of sleep: (1) maintenance of distinct postures at specific environmental locations, (2) loss of locomotion, (3) rapid reversibility to wake, (4) enhanced arousal thresholds to environmental stimuli, and (5) homeostatic regulation[1,2].

Arousal states in mammals and birds can be roughly distinguished into three stages based on electroencephalogram (EEG) and electromyography (EMG): wakefulness, non-rapid eye movement sleep (non-REM sleep), and rapid eye movement sleep (REM sleep) (Fig. 1).

Invertebrates also exhibit sleep. Fruit flies (*Drosophila melanogaster*) rest under a circadian rhythm. This state of low activity fits the definition of sleep[1]. Nematodes (*Caenorhabditis elegans*) exhibit two different states that fit the definition of sleep. After hatching, nematodes undergo four molts and become adults in approximately 3 days. Nematodes always exhibit a motionless state called lethargus (developmentally-timed sleep) 2–3 hours before molting[3]. In addition, nematodes show an immobile state after stress, such as exposure to heat or ultraviolet[4,5]. Two neurons are critical for nematode's sleep; the ring interneuron S (RIS) neuron is important for regulating developmentally-timed sleep, and the anterior lateral A (ALA) neuron is crucial for the induction of stress-induced sleep[6]. However, the molecular pathways involved in regulating sleep and to what extent they are conserved among vertebrates and invertebrates remain largely unknown.

In humans, natural short sleepers exhibit a reduced amount of time in sleep without reporting daytime fatigue[7]. In cases where the natural short-sleep trait is hereditary, identifying the causal gene is expected to lead to understanding the molecules that control sleep homeostasis and may provide clues to understanding the mechanisms that define sleepiness. The mechanisms defining sleepiness are related to the

functional aspects of sleep. The short-sleeper causative gene may provide clues to understanding the mystery in sleep research: why we sleep. Natural short sleep-related genes have been explored over the years. By analyzing the sleep/wake cycle of mutant mice, several short sleep-related genes have been found. Mutations in *DEC2*, *ADRB1*, *NPSR1*, and *GRM1*, which were found from the human short-sleeper family lineage, lead to a short-sleep phenotype in mice[8–11]. *Dec2* encodes a transcription factor that is involved in the regulation of the circadian rhythm[8]. The mutation found in natural short sleepers converts proline into arginine at position 385 (P385R) of DEC2. *Adrb1* encodes the β1-adrenergic receptor[9]. The mutation found in natural short sleepers converts alanine into valine at position 187 (A187V) of ADRB1. *Npsr1* encodes the neuropeptide S receptor[10]. The mutation found in natural short sleepers converts tyrosine into histidine at position 206 (Y206H) in both known isoforms. *Grm1* encodes the metabotropic glutamate receptor 1[11]. Two mutations have been found in this gene in human short-sleeper families. One mutation converts arginine into tryptophan at position 889 (R889W) in the C-terminal intracellular domain of the isoform mGluR1b. Another mutation converts serine into alanine at position 458 (S458A). In addition, *Nr3a*, an NMDA receptor gene, leads to a short-sleep phenotype when deleted in mice[12]. Moreover, two muscarinic acetylcholine receptor genes (*Chrm1* and *Chrm3*) are for REM sleep regulation. Double KO mice of these two genes have been shown to have an almost complete loss of REM sleep and reduced non-REM sleep[15]. In addition, KO mice of *Slc6a3*, which encodes the dopamine transporter, exhibit decreased non-REM sleep, likely due to increased extracellular dopamine levels[13]. Thus, several genes whose mutations cause short sleep have been found. However, their effects are mild (up to 25%). Mutant mice showing severe sleep loss (over 50%, similar to extreme short sleepers in humans) have not been previously reported, and there may be yet unidentified genes that control the sleep/wake cycle.

In addition, recent studies using invertebrate animal models suggest that sleep-regulatory mechanisms are at least partly conserved at the molecular level between vertebrates and invertebrates[1]. For example, a gain-of-function mutation in the salt-inducible kinase 3 (*Sik3*) leads to a drastic increase in the amount of non-REM sleep in

mice, whereas its orthologue in the nematodes promotes developmentally-timed sleep and total sleep in fruit flies[14]. Thus, studies using invertebrate animal models are also expected to identify key molecules that contribute to sleep regulation across the animal phyla.

AP-2 transcription factor family (TFAP-2)

AP-2 transcription factors and sleep

In this study, I focused on the transcription factor AP-2β (TFAP2B).

In humans, mutations in TFAP2B lead to Char syndrome[15, 16]. Two human kindreds with Char syndrome (kindred 144 and 145), containing members of both sex, have self-reported abnormalities in sleep, namely parasomnia (sleep-walking) and short sleep, respectively[17]. In patients with non-REM sleep parasomnias (including sleep-walking syndrome), non-REM sleep-like patterns are observed in the frontal association cortex and hippocampus, and wake-like patterns in the motor cortex and emotion-related areas during parasomnias episodes[18]. These kindreds carried heterozygous mutations located in the predicted splice donor just after the sequence of exon 3 in the gene (K144, Fig. 2A, B) and predicted splice acceptor just before the sequence of exon 5 in the gene (K145, Fig. 2A, C)[17], thus implying the involvement of TFAP2B in sleep regulation.

In nematodes, the orthologue transcription factor APTF-1 is crucial for the specification of the sleep-promoting RIS neuron, and *aptf-1* mutants exhibit severely reduced quiescence during both developmentally-timed sleep and stress-induced sleep[6,19, 20]. In addition, in the fruit fly, knockdown of neuronal TFAP2 results in reduced night-time sleep[21]. However, invertebrate sleep analysis methods are primarily based on movement and not on brain activity from EEG. The nematode *aptf-1* mutant may exhibit a parasomnia-like phenotype. In other words, the *Tfap2b* mutant needs to be analyzed for sleep/wake cycles based on EEG data using mammals.

TFAP2B is a member of the AP-2 transcription factor family. The AP-2 transcription factor family (TFAP-2) is conserved in various species, from nematodes to humans. There are five TFAP-2 proteins in humans and mice: TFAP2A, TFAP2B, TFAP2C, TFAP2D, and TFAP2E. A highly conserved helix-span-helix dimerization motif at the

carboxyl terminus is used to form heterodimers and homodimers[22]. The basic domain in the middle region binds to DNA with the helix-span-helix motif. The proline- and glutamine-rich region at the amino terminus acts as a transcriptional activator. TFAP-2 family proteins can bind to the palindrome sequence 5′ -GCCN$_3$GGC-3′. Many genes with TFAP-2 binding sites in their promoter regions are associated with biological phenomena such as cell development and differentiation[23]. In addition, palindromic sequences are observed in the cis-element of tyrosine hydroxylase, which is important for the production of dopamine, and dopamine beta-hydroxylase, which is important for the production of noradrenaline, suggesting that the TFAP-2 family is involved in the transcription of these genes[24].

Tfap2b is located on chromosomes 6 and 1 of humans and mice, respectively, and comprises seven exons (NCBI Gene ID: 21419). The coding sequences of mouse Tfap2b and human TFAP2B are more than 90% identical. *Tfap2b* is expressed in neural crest cells and subsequently in parts of the brain throughout embryonic and early development. In mice, *Tfap2b* KO pups die shortly after birth due to renal failure[25, 26]. *Tfap2b* has also been implicated in limb formation[27], differentiation of some neurons[28-31], obesity[32], and glaucoma[33]. In humans, *TFAP2B* mutation causes Char syndrome (MIM 169100)[15], a congenital disease characterized by patent ductus arteriosus, facial dysmorphism, and hand anomalies[16].

Aim of my study: Analysis of the roles of TFAP2B in sleep regulation in mice

In combination with recent studies supporting the view that the molecular mechanisms of sleep are conserved between mammals and invertebrates, I expected that mammalian TFAP2B may be involved in sleep regulation. However, in mammals, conclusive evidence is lacking because the direct effect of mutating this gene is unknown. Thus, in this study, I aimed to elucidate the effects of mutating *Tfap2b* in mice.

Materials and Methods

Animals

All animal experiments were approved by the institutional animal care and use committee of the University of Tsukuba. All animals were maintained according to the institutional guidelines of the animal facilities of the Laboratory of Animal Resource Center, University of Tsukuba. Mice were maintained and bred in International Institute for Integrative Sleep Medicine under a 12-hour light/dark cycle and free access to food and water. Male *Tfap2b*$^{K144/+}$, *Nestin-Cre;Tfap2b*$^{flox/flox}$, male and female *Tfap2b*$^{K145/+}$, *Tfap2b*$^{+/-}$ mice, and corresponding control mice aged 10–13 weeks were used for sleep analyses.

To obtain *Tfap2b*$^{+/-}$ mice, *Tfap2b*$^{tm1a(EUCOMM)Wtsi/+}$ mice from KOMP (Knockout Mouse Project)[34] were crossed with mice carrying the *Ayu1-Cre* allele[35] to remove a genomic DNA fragment containing *Tfap2b* exon 3 and a neomycin-resistant cassette flanked by *loxP*. The *Tfap2b*$^{tm1a(EUCOMM)Wtsi}$ allele contains an *IRES:lacZ* trapping cassette with *Engrailed* (En2) splice acceptor sequences immediately after *Tfap2b* exon 2 and is followed by a poly-A transcription termination signals. F1 offspring were then maintained by crossing with C57BL/6J mice.

To obtain *Tfap2b* conditional KO mice, *Tfap2b*$^{tm1a(EUCOMM)Wtsi/+}$ mice were crossed with mice carrying the *CAG-flp* allele[36] to remove a genomic DNA fragment containing *IRES:lacZ* and a neomycin-resistant cassette flanked by *FRT*. Homozygous floxed *Tfap2b* exon 3 (*Tfap2b*$^{flox/flox}$) mice were mated to mice carrying the *Nestin-Cre* allele[37] to induce nervous system-specific recombination.

To confirm the recombination sites in the *Nestin-Cre* mice, *Nestin-Cre* mice were mated with the GFP reporter strain B6.129S4-*Gt(ROSA)26Sor*$^{tm1(CAG-EGFP/Rpl10a,-birA)Wtp}$/J (*Rosa26* $^{LSL-L10-GFP}$, Jackson Laboratory).

Tfap2b^{K144} and *Tfap2b*^{K145} mice were generated using CRISPR/Cas9 technology by Dr. Tomoyuki Fujiyama, Dr. Nanae Nagata, Dr. Taizo Kawano, Dr. Seiya Mizuno, Dr. Fumihiro Sugiyama, Dr. Satoru Takahashi. I amplified the genomic region, including the target sites and PAM sequence, by PCR with the following primers and confirmed the insertion of the desired mutation and the absence of additional mutations.

Tfap2b^{K144}: 5′-AAAACCTCCATTTGTGGGTTAAT-3′ & 5′-TGCCAGTGTTGCTCTGATCT-3′; *Tfap2b*^{K145}: 5′- TCTGGATCCACTGCCCTAAC-3′ & 5′-CACTCATAAGGGCACAGCAA-3′. F0 mice were mated with wild-type (WT) C57BL/6J mice for at least four generations before sleep recording.

Genotyping

Genotyping of *Tfap2b*$^{+/-}$, *Tfap2b*$^{flox/flox}$, *Nestin-Cre*, *Rosa26* $^{LSL-L10-GFP}$ mice was performed using the following primers, *Tfap2b*$^{+/-}$: 5′-GACATCCTACAATGCACAGCT-3′, 5′-CAACGGGTTCTTCTGTTAGTCC-3′, & 5′-TTGCTGTGAGCTAAGAGCTTC-3′ (WT: 381 bp, *Tfap2b*$^{-}$ mutant: 529 bp), *Tfap2b*$^{flox/flox}$ 5′-AAGGCGCATAACGATACCAC-3′, & 5′-CCGCCTACTGCGACTATAGAGA-3′ (*Tfap2b*^{flox}: 218 bp), *Nestin-Cre*: 5′-GACGATGCAACGAGTGATGA-3′, & 5′-AGCATTGCTGTCACTTGGTC-3′ (*Nestin-Cre*: 300 bp). *Rosa26* $^{LSL-L10-GFP}$: 5′-AAGGGAGCTGCAGTGGAGTA-3′ &5′-CCGA AAATCTGTGGGAAGTC-3′ & 5′- AAGATCCGCCACAACATCG-3′, TTCTCGTTGGGGTCTTTGCT-3′ (*Rosa26* $^{LSL-L10-GFP}$: 146 bp).

For routine genotyping of *Tfap2b*^{K145} and *Tfap2b*^{K144}, I applied the derived cleaved amplified polymorphic sequences (dCAPS) [38] method using the following combinations of primer pairs and restriction enzymes. *Tfap2b*^{K144}: 5′-AAAACCTCCATTTGTGGGTTAAT-3′ & 5′-AGACATTGAAATCTTTGCTTACTTTTGGAAGAAAGGATC-3′ followed by digestion by *Bam*HI to specifically digest the WT allele (WT: 183 bp, *Tfap2b*^{K144} mutant: 223 bp). *Tfap2b*^{K145}: 5′-GAATGTTAATTCTCACCAGTGCA-3′ & 5′-CACTCATAAGGGCACAGCAA-3′ followed by digestion by *Apa*LI to specifically digest the mutant allele (WT: 266 bp, *Tfap2b*^{K145} mutant: 247 bp).

Reverse transcription (RT)-PCR

The brains of mouse embryos were harvested 18 days after detection of vaginal plugs (embryonic day 18.5; E18.5). Each brain was divided in half at the midline and frozen with liquid nitrogen. Samples of brains of mixed sex were used. Total RNA was extracted from the samples using TRIzol reagent (ThermoFisher). Genomic DNA was

digested, and reverse transcription was performed with oligo-dT and random primers using QuantiTect Reverse Transcription Kit (Qiagen). RT-PCR was performed using the following primers.

Tfap2b: 5′-CGACAGCCTCTCGTTGCA-3′ & 5′-TGCTGTCTGTTCAAATACTCGGA-3′ (WT: 543 bp, *Tfap2b*^{K144}: 543 bp, *Tfap2b*^{K145} long: 541 bp, *Tfap2b*^{K145} short: 424 bp). *Rpl23*: 5′-TTCCGGTCGGAGCTGTGAT-3′ & 5′-CTGCTGGATGTACCTTTTTCCTT (WT: 180 bp). PCR products were purified and subjected to direct sequencing. For *Tfap2b*$^{K145/K145}$, which resulted in PCR products of two different sizes, each of which was purified by gel extraction.

Western blots

Western blots were performed as previously reported[14], with some modifications. The brain samples were harvested from E18.5 mice by RT-PCR. Tissues were homogenized in ice-cold lysis buffer [20 mM HEPES, pH 7.5, 100 mM NaCl, 10 mM $Na_4P_2O_7$, 1.5% Triton X-100,15 mM NaF, 1x PhosSTOP (Roche), 5 mM EDTA, 1x protease inhibitor (Roche)], and then centrifuged at 14,000 rpm at 4°C. The supernatants were adjusted for 2.5 μg/μL by SDS sample buffer, then boiled at 95°C for 5 minutes and stocked at -30°C. The samples were boiled at 95°C for 5 minutes and then separated by SDS–PAGE and transferred to the polyvinylidene difluoride membrane. The primary antibody was 1/500 rabbit anti-TFAP2B (Atlas Antibodies; Cat. No. HPA034683) dissolved in 5% skim milk tris-buffered saline with Tween20 (TBST; 50 mM Tris-HCl, pH 7.6, 150 mM NaCl, 0.05% Tween20). The second antibody was 1/5,000 horseradish peroxidase (HRP)-conjugated donkey anti-rabbit IgG (Jackson ImmunoReserarch; Cat. No. 711-035-152) or 1/2,000 HRP-conjugated donkey anti-rabbit IgG (Abcam; Cat. No. ab7083) dissolved in 5% skim milk TBST. Clarity Western ECL Substrate (Bio-Rad) or Chemi-Lumi One Super (Nacalai Tesque) were used to develop chemiluminescence. The illumination was detected by fusion SOLO5 (Vilber-Lourmat). Then antibodies were stripped by incubating WB Stripping Solution Strong (Nacalai Tesque). For detecting ß-tubulin as an internal control, rabbit anti-ß-tubulin (CST; Cat. No. 2128) dissolved in

5% bovine serum albumin TBST and HRP-conjugated donkey anti-rabbit IgG were used as the primary and secondary antibody.

Sleep recording

EEG and EMG signals were recorded from freely moving mice at the age of 8–13 weeks according to the method described in a previous study[39], with some modifications. In addition, 8–10 week-old mice were implanted with the EEG/EMG electrodes. Stainless EEG electrodes were implanted epidurally over the cerebellum and the parietal cortex, and EMG electrodes were embedded into the trapezius muscles bilaterally. At least 4 days after surgery, mice were introduced to the sleep recording chamber and habituated for at least 5 days. Subsequently, EEG/EMG signals were recorded from the onset of the light phase. EEG/EMG signals were filtered [EEG: bandpass 0.5–64 Hz (sampling rate: 128 Hz) or 0.5–250 Hz (sampling rate: 512 Hz), EMG: bandpass 10–40 Hz], collected, and digitized at a 128 or 512 Hz sampling rate using VitalRecorder (Kissei Comtec). Video and infrared signals were also recorded from the start of the light phase. These were used to check for changes in activity.

Sleep analysis

EEG/EMG data were divided into 4-s epochs (time window), and EEG data were further subjected to fast Fourier transform analyses using SleepSign (Kissei Comtec). The vigilance state in each epoch was manually classified as REM sleep, non-REM sleep, or wake based on absolute delta (0.5–4 Hz) power, theta (6–10 Hz) power to delta power ratio, and the integral of EMG signals. If a single epoch contained multiple states, the state with the highest occupancy was assigned. The EEG power spectrum of each state was calculated and normalized by EEG power at 16–30 Hz averaged across 24 hours[40]. Epochs that contained multiple stages or presumable large movement-derived artifacts in the EEG data were included in the stage analysis but excluded from the EEG power spectrum analysis. In addition, only the EEG/EMG data collected at 512 Hz were included in the EEG power spectrum analyses.

Activity recording

Mice were habituated to the recording cage for at least 1 week and entrained to the 12-hour light/dark cycle for 7 days. Then they were put under dark/dark conditions for 7 days. Wheel revolutions and the motion detected by the infrared sensor were recorded in 5 minute bins and analyzed with ClockLab analysis software (Actimetrics).

Histology

Deeply anesthetized mice were killed by injecting a lethal dose of anesthetic and underwent transcardial perfusion with 0.1 M phosphate-buffered saline (PBS) followed by 4% paraformaldehyde (w/v) in 0.1 M PBS or 10% formalin neutral buffer solution. The brains were postfixed in the same fixative for 2 hours for X-gal staining and 1 day for DAPI staining and subsequently equilibrated in 30% sucrose (w/v) in PBS. The brains were sectioned at 40 μm using a sliding microtome (Yamato Kohki) or a cryostat (Leica).

X-gal staining

After washing with PBS, the sections were incubated in 5-bromo-4-chloro-3-indolyl-ß-galactopyranoside (X-gal) staining solution (0.05% X-gal, 1 mM $MgCl_2$, 3 mM $K_4Fe(CN)_6$, 3 mM $K_3Fe(CN)_6$, and 0.1% Triton X-100 in PBS) at 37°C. The sections were mounted on a slide glass, counterstained with Nuclear Fast Red (Vector Laboratories; H-3403-500) covered with Entellan New (Merck; 107961). The images were captured with a digital slide scanner (Hamamatsu; NanoZoomer).

DAPI staining

Sections were washed in TBST, then incubated with DAPI. After washing in TBST, the sections were mounted on a slide glass with mounting medium (ThermoFisher; TA-006-FM). DAPI and GFP signals were detected with a digital slide scanner (Carl Zeiss; AxioScan.Z1).

Statistics

I was blinded to the genotype during sleep scoring. All statistical analyses were performed using Prism8 and Prism9 (GraphPad), and statistical significance was set at $p < 0.05$. Where applicable, all statistical tests were two-tailed.

Results

Generating *Tfap2b* mutant mice that mimic human kindred 144 and 145

I aimed to generate mice that carry mutations in *Tfap2b* (MGI:104672), which mimic the mutations in the human kindreds 144 and 145. In kindred 144, a single base substitution (G to A) at position +5 of the splice donor site of intron 3 was detected (TFAP2B c.601+5G>A), whereas in kindred 145, a single base substitution (G to C) in the splice acceptor site of intron 4 immediately before exon 5 (TFAP2B c.822-1G>C) was detected (Fig. 2A-C)[17]. The genomic DNA sequences around both sites were highly conserved between humans and mice (Fig. 2B, C). Using the CRISPR/Cas9 system, point mutations were introduced in mice corresponding to the mutations in human kindred 144 and 145 (hereafter, *Tfap2b*^{K144} and *Tfap2b*^{K145}, respectively) (Fig. 2B, C). The genomic DNA sequences around the targeted sites in *Tfap2b*^{K144} and *Tfap2b*^{K145} were further confirmed by direct sequencing, and dCAPS were applied for genotyping of the *Tfap2b* alleles (Fig. 3A-D).

I checked the effects of these mutations on the *Tfap2b* mRNA sequence around exon 3–5, where abnormal splicing due to these mutations is predicted to occur by RT-PCR (Fig. 4A) and direct sequencing (Fig. 5). Considering that homozygous *Tfap2b* KO mice die shortly after birth[25, 26], brain samples were collected from the embryos just before birth (embryonic day 18.5; E18.5). Consequently, I detected no abnormal splicing in *Tfap2b*$^{K144/K144}$ mice (Fig. 4A, Fig. 5). By contrast, *Tfap2b*$^{K145/K145}$ mice showed very low expression levels of *Tfap2b* mRNA (Fig. 4A), and mRNAs of two different lengths were detected (Fig. 4B). In the longer mRNA, two nucleotides at the 5′-end of exon 5 were deleted. In the shorter mRNA, exon 5 was completely deleted (Fig. 5), likely due to exon skipping. Both variants of *Tfap2b* mRNA in *Tfap2b*$^{K145/K145}$ mice are predicted to lead to a frameshift that results in a premature stop codon.

Next, I checked the effects of these mutations on the TFAP2B protein expression level and molecular weight by Western blot using an antibody that recognizes TFAP2B at the region encoded in exon 2. Similar to the above RT-PCR, brain samples were

collected from the embryos just before birth (E18.5). I also applied a *Tfap2b* KO allele (*Tfap2b*$^{-}$), in which exon 3 is deleted, and poly-A transcriptional termination signals are inserted just after exon 2[34] to the analysis. The protein expression level was reduced to about half in *Tfap2b*$^{+/-}$ mice and was further reduced in *Tfap2b*$^{-/-}$ mice (Fig. 4C). Although exon 1 and exon 2 are intact in *Tfap2b*$^{-}$, no additional bands were detected in samples derived from *Tfap2b*$^{+/-}$ or *Tfap2b*$^{-/-}$ mice, suggesting that the expression level of the truncated TFAP2B protein is very low if any. In contrast, I detected no effects in *Tfap2b*$^{K144/+}$ and *Tfap2b*$^{K144/K144}$ mice (Fig. 4D). Concerning the *Tfap2b*^{K145} allele, while no obvious effects were detected in *Tfap2b*$^{K145/+}$ mice, *Tfap2b*$^{K145/K145}$ mice exhibited a significant decrease in the protein expression level that was comparable to *Tfap2b*$^{-/-}$ mice (Fig. 4E). Consistently, I never obtained *Tfap2b*$^{K145/K145}$ pups, suggesting that the condition is lethal. Similar to the other *Tfap2b* alleles, I detected no additional bands produced by the *Tfap2b*^{K145} allele.

Tfap2b$^{+/-}$ female mice show increased wakefulness and decreased non-REM sleep

To test the involvement of *Tfap2b* in sleep regulation, I first compared the sleep architecture between WT and *Tfap2b*$^{+/-}$ mice. The total time spent in wakefulness, non-REM sleep, or REM sleep was not significantly different between male WT and *Tfap2b*$^{+/-}$ littermates (Fig. 6A, B). The duration and number of episodes of wakefulness and non-REM sleep were not significantly altered either (Fig. 7A, B). The episode number of REM sleep was slightly increased (Fig. 7A).

In contrast, when I compared sleep between female WT and their *Tfap2b*$^{+/-}$ littermates, total time spent in wakefulness was increased, and that in non-REM sleep was decreased (Fig. 6D). REM sleep was not significantly different (Fig. 6D). When light and dark phases were separately analyzed, I did not detect any interaction between time of the day and the amount of wakefulness or non-REM sleep, but a main effect of genotype was detected, suggesting that the amount of wakefulness and non-REM sleep are affected across the whole day in female *Tfap2b*$^{+/-}$ mice (Fig. 6C, D). Episode analyses revealed that the duration of wakefulness was increased in the dark

phase, which might partly account for the increased amount of wakefulness (Fig. 7D). The duration and number of episodes of REM sleep and non-REM sleep were not significantly altered (Fig. 7C, D). When the EEG power spectrum in each stage across 24 h and the bi-hourly changes in delta density during non-REM sleep were analyzed, female *Tfap2b*$^{+/-}$ mice showed a trend for decreased delta power during non-REM sleep, although not significant (Fig. 8B; Fig. 8D). Male *Tfap2b*$^{+/-}$ mice exhibited a slight increase in the EEG power of approximately 4–4.5 Hz during non-REM sleep which might have resulted from a slight shift in the peak frequency (Fig. 8A).

Tfap2b$^{K145/+}$ female mice show fragmented non-REM sleep

Considering that the TFAP2B protein expression level and survival rate were severely affected in *Tfap2b*$^{K145/K145}$ mice, I examined the sleep architecture of *Tfap2b*$^{K145/+}$ male and female mice. Similar to male *Tfap2b*$^{+/-}$ mice, total time spent in wakefulness, non-REM sleep, or REM sleep in *Tfap2b*$^{K145/+}$ male mice were not significantly different from WT littermates (Fig. 9A, B). The episode duration and number of each state were also not significantly affected (Fig. 10A, B). During REM sleep, EEG power in the theta range was slightly reduced (Fig. 11A).

Total time spent in wakefulness, non-REM sleep, or REM sleep was also not significantly affected in female *Tfap2b*$^{K145/+}$ mice (Fig. 9C, D). However, in contrast to female *Tfap2b*$^{+/-}$ mice, the episode number of wakefulness, non-REM sleep, and REM sleep was increased during the light phase (Fig. 10C). In addition, the duration of episodes of non-REM sleep was largely decreased (Fig. 10D). These results suggested that the sleep/wake stages were fragmented in the female *Tfap2b*$^{K145/+}$ mice, especially the non-REM sleep in the light phase. The EEG power spectra and non-REM sleep delta density were not significantly affected (Fig. 11B; Fig. 11D).

Tfap2b$^{K144/+}$ mice show reduced non-REM sleep in the dark phase

Next, I compared the sleep architecture between male WT and their *Tfap2b*$^{K144/+}$ littermates. *Tfap2b*$^{K144/+}$ mice exhibited a significant decrease in the time spent in non-

REM sleep, specifically in the dark phase (Fig. 12A, B). This was likely accounted for by a trend for a decreasing number of non-REM sleep episodes (Fig. 12C). In addition, during the dark phase, the episode duration of wakefulness was significantly increased, suggesting that each wake episode is more consolidated (Fig. 12D). The EEG power spectra and non-REM sleep delta density were not significantly affected (Fig. 13A, B).

Nervous system-specific *Tfap2b* deletion induces decreased non-REM sleep and increased wakefulness

The deficiency in TFAP2B affected sleep in mice. To further elucidate whether TFAP2B functions in the nervous system or in other tissues, I used *Nestin-Cre* mice to induce nervous system-specific KO of *Tfap2b*. The homozygous *Tfap2b* KO mice die shortly after birth[18], but the nervous system-specific homozygous *Tfap2b* KO (*Nestin-Cre; Tfap2b*$^{flox/flox}$), in which exon 3 is deleted in Cre-expressing cells resulting in a frameshift that generates a premature stop codon immediately after the start site of exon 4, were alive to adult. I compared the sleep architecture between *Tfap2b*$^{flox/flox}$, *Nestin-Cre; Tfap2b*$^{flox/+}$, and *Nestin-Cre; Tfap2b*$^{flox/flox}$ male mice. *Nestin-Cre; Tfap2b*$^{flox/flox}$ showed a significant increase in the total time spent in wakefulness and the expense of the total time spent in non-REM sleep, as compared with *Tfap2b*$^{flox/flox}$ and *Nestin-Cre; Tfap2b*$^{flox/+}$ littermates (Fig. 14A). The episode duration of wakefulness was increased (Fig. 14B). However, episode numbers of wakefulness and non-REM sleep decreased (Fig. 14C). *Nestin-Cre; Tfap2b*$^{flox/flox}$ mice exhibited an increase in the EEG power approximately 5.5–17 Hz during wakefulness (Fig. 15). Observations of individual sleep/wake cycles showed that *Nestin-Cre; Tfap2b*$^{flox/flox}$, unlike *Tfap2b*$^{flox/flox}$ and *Nestin-Cre; Tfap2b*$^{flox/+}$, did not initiate activity at the onset of the dark period (Fig. 16A-C). Therefore, I examined the eye of *Nestin-Cre; Tfap2b*$^{flox/flox}$ mice and discovered that it looked opaque (Fig. 17A). Neural crest-specific deletion of *Tfap2b* has been reported to induce glaucoma[25] and that the photosensitive interneurons are affected in conditional *Tfap2b* KO mice[21]. Bodyweight was also affected in *Nestin-Cre; Tfap2b*$^{flox/flox}$ mice (Fig. 17B). I analyzed the behavioral rhythms of several mice by monitoring wheel-running activity and found that *Nestin-Cre; Tfap2b*$^{flox/flox}$ mice did

not show a coincidence between the onset of activity and the onset of the dark period under 12L:12D (LD) entraining condition (Fig. 18A-C), suggesting that the light sensitivity of these mice may be affected.

Tfap2b is expressed in the superior colliculus, parabrachial nucleus, locus coeruleus, cerebellum, and nucleus of solitary tract

The *Tfap2b*$^{-}$ allele used in this study harbors a LacZ-expressing cassette that replaces the original *Tfap2b* gene (Fig. 19A), thus allowing us to investigate the expression pattern of *Tfap2b* by X-gal staining. X-gal signals were observed in the hypothalamus, midbrain, and hindbrain (Fig. 19B-F). Strong X-gal signals were observed in the superior colliculus (SC; Fig. 19C'), parabrachial nucleus (Pb; Fig. 19D'), cerebellum (Fig. 19E'), locus coeruleus (LC; Fig. 19E"), and the nucleus of solitary tract (NTS; Fig. 19F'), whereas weak signals were detected around the paraventricular hypothalamic nucleus (PVH; Fig. 19B'). No signals were detected in the other areas, including the olfactory bulb, cerebral cortex, and preoptic area. To confirm the recombination sites by *Nestin-Cre*, I crossed these mice with *Rosa26* $^{LSL\text{-}L10\text{-}GFP}$ mice. I checked the PVH, SC, Pb, cerebellum, LC, NTS and the site observed the X-gal signals. *Nestin-Cre; Rosa26* $^{LSL\text{-}L10\text{-}GFP/+}$ mice showed GFP signals in SC, Pb, cerebellum, and NTS but less in PVH and LC (Fig. 20A'-E').

Discussion

The transcription factor AP-2 plays essential roles in developmentally-timed sleep or stress-induced sleep in nematodes[6,19, 20] and daily sleep in fruit flies[21], suggesting the conserved involvement of this factor in invertebrate sleep. However, the roles of AP-2 in mammalian sleep remain unknown. The current study provides direct evidence showing that the deficiency in TFAP2B affects sleep in mice. These studies strongly suggest a highly conserved role of the molecular pathway involving TFAP2B in sleep between mammals and invertebrate animals. Moreover, the current study revealed that mutations in the intron of *Tfap2b* mimicking mutations that were identified in human kindreds with Char syndrome affect sleep in a manner that is largely different from each other or from *Tfap2b* deficiency. Thus, this study provides an important example showing that mutations in a single gene can result in diverse sleep phenotypes, which might explain the diverse nature of sleep-related symptoms in Char syndrome or other familial diseases. My findings reveal that *Tfap2b*$^{+/-}$ female mice exhibit reduced non-REM sleep and increased wakefulness amounts. This is consistent with the effect of deleting or knocking down the orthologues in nematode or fly and supports the notion that the molecular mechanism of mammalian non-REM sleep and invertebrate sleep are conserved[1]. It remains unclear why male *Tfap2b*$^{+/-}$ mice did not exhibit significantly reduced non-REM sleep, although a trend was observed. Female and male mice have similar sleep homeostatic properties, but females show less sleep amount than that of males, and several environmental factors can affect their sleep differently, suggesting some sex differences in the sleep regulation mechanisms[41]. *Tfap2b* deficiency might have affected a sleep-regulatory pathway that is more vulnerable in females. Although the effect of the estrous cycle on sleep in females remains a concern, in case of the C57BL/6J mice used in this study, the estrous cycle has no significant effect on the amount of non-REM sleep and wakefulness[42].

In contrast to *Tfap2b*$^{+/-}$ mice, *Tfap2b*$^{K145/+}$ female mice did not exhibit reduced non-REM sleep amount but instead exhibited fragmented non-REM sleep. The TFAP2B protein expression level was decreased to a similar extent in *Tfap2b*$^{-/-}$ and

Tfap2b$^{K145/K145}$ mice. *Tfap2b*^{K145} harbors a single base substitution within the highly conserved splice acceptor sequence (AG) immediately before exon 5. Thus, *Tfap2b*^{K145} was predicted to lead to the skipping of exon 5[17]. Indeed, in the *Tfap2b*$^{K145/K145}$ mice, I detected a shortened *Tfap2b* mRNA in which exon 5 was missing. I also detected a *Tfap2b* mRNA in which only two nucleotides at the 5′ -end of exon 5 were deleted. In both cases, the variation in the mRNA sequence leads to a frameshift that results in a premature stop codon. The predicted protein size of the mRNA lacking exon 5 is 31 kDa and that of the mRNA lacking the first two bases of exon 5 is 36 kDa. These proteins are likely nonfunctional. The mRNA expression level was also largely decreased in the *Tfap2b*$^{K145/K145}$ mice, likely due to nonsense-mediated decay. Moreover, the 31 kDa and 36 kDa bands were not detected by Western blotting. Regarding the WT size band of *Tfap2b*$^{K145/K145}$, the sample used in Western blotting were embryonic brains, which might have been contaminated with maternal samples. Bands of similar intensity were seen in the *Tfap2b*$^{-/-}$ samples, which might also be of maternal origin. Another possibility is that the antibody weakly binds to the other four TFAP-2 family members, which have molecular weights of 46–50 kDa, similar to WT TFAP2B. However, I consider this unlikely, because the homology of the amino acid sequence of the antibody recognition site with the other four TFAP-2 family members is low, although I cannot completely exclude this possibility. While Western blot showed that the TFAP2B protein expression level was largely decreased in *Tfap2b*$^{K145/K145}$ mice, it remains unknown why *Tfap2b*$^{K145/+}$ and *Tfap2b*$^{+/-}$ mice exhibit totally different sleep phenotypes. Unlike *Tfap2b*$^{+/-}$ mice, *Tfap2b*$^{K145/+}$ mice did not exhibit an obvious reduction in TFAP2B protein, which may result from enhanced transcription of the WT allele by mechanisms of transcriptional adaptation[43]. In addition to nonsense-mediated decay, *Tfap2b*^{K145} might cause some effect on the protein that is different from *Tfap2b*$^{-}$. For example, a small proportion of the mRNA derived from *Tfap2b*^{K145} may be translated, resulting in the expression of an abnormal protein that interferes with the function of the WT TFAP2B protein, such as the gain-o- function effect. However, no additional short bands were detected in the Western blot. The amount of such abnormal protein is expected to be very low.

The sleep phenotype of *Tfap2b*$^{K144/+}$ mice also differed from the other *Tfap2b* mutants. Male *Tfap2b*$^{K144/+}$ mice showed reduced non-REM sleep during the dark phase. *Tfap2b*^{K144} harbors a single base substitution within the putative splice donor sequence immediately after exon 3. In human cells, *in vitro* experiments suggest that this mutation leads to the skipping of exon 3[17]. If exon 3 is skipped in *Tfap2b*^{K144}, it will cause a frameshift and premature termination codon, which would lead to either the production of a truncated protein or nonsense-mediated decay of the mRNA. However, in the case of the *Tfap2b*^{K144} allele, I detected no effects on the *Tfap2b* mRNA expression level nor sequence. Moreover, I detected no effects on the TFAP2B protein expression level nor the molecular weight even in homozygotes. In addition, unlike *Tfap2b*$^{K145/K145}$ mice, *Tfap2b*$^{K144/K144}$ mice were viable. Thus, further analyses are required to determine how the mutation affects the properties of TFAP2B. Furthermore, considering that cis-elements of transcriptional regulation can exist in introns, *Tfap2b*^{K144} may affect the expression pattern of *Tfap2b*.

While this study successfully showed that mutations in *Tfap2b* can differently affect sleep, the effects of *Tfap2b*^{K144} and *Tfap2b*^{K145} on mouse sleep did not match the sleep-related symptoms that were self-reported by human kindreds 144 and 145. In humans, kindred 144 self-reported parasomnias. However, although I monitored mice behaviors by video and EEG/EMG recording, I observed no abnormal movements during sleep in any of the *Tfap2b* mutants. In addition, kindred 145 self-reported short sleep, whereas *Tfap2b*$^{K145/+}$ mice exhibited fragmented sleep. The effects of the mutations in *Tfap2b* may differ depending on the species or other genetic backgrounds. In addition, the human studies on kindreds 144 and 145 did not include polysomnography; thus, the self-reports on sleep might have been inaccurate.

The homozygous *Tfap2b* KO mice die shortly after birth[25, 26], but the nervous system-specific homozygous *Tfap2b* KO mice were alive to adulthood. Not only renal failure but also noradrenaline deficiency has been suggested as the cause of lethality[30]. *Nestin-cre* did not induce the Cre recombination at LC, suggesting the LC neurons produce noradrenaline normally at *Nestin-Cre; Tfap2b*$^{flox/flox}$ mice. Noradrenaline deficiency does not occur in the central neuronal system, and *Nestin-Cre; Tfap2b*$^{flox/flox}$

may have survived to adulthood. *Nestin-Cre; Tfap2b*$^{flox/flox}$ male mice showed a decrease in the number of episodes of wakefulness, but an increase in the duration of wakefulness, resulting in an increase in the total amount of wakefulness. Moreover, it exhibited a decrease in the number of episodes of non-REM sleep, resulting in a decrease in the total amount of non-REM sleep.

In the adult brain, *Tfap2b* expression was detected in the SC, Pb, LC, cerebellum, and NTS. Within these areas, the SC is implicated in the acute induction of sleep triggered by light stimulation during the dark phase, although its dysfunction does not affect baseline sleep[44]. By contrast, LC contains wake-promoting neurons[45], and global or local deletion of dopamine ß-hydroxylase, essential for the synthesis of noradrenalin in LC, results in reduced wakefulness and increased non-REM sleep[46, 47]. Thus, although deletion of *Tfap2b* leads to reduced expression of dopamine ß-hydroxylase in the LC[30], it requires further investigation whether it can explain the observed sleep phenotypes in this study.

Other possibilities include the involvement of TFAP2B expressed in the Pb and NTS in sleep regulation, considering that the Pb is important for maintaining wakefulness and that Pb lesions lead to increased amounts of sleep [48], NTS is important in the formation of the sleep/wake cycle, and NTS lesions lead to insomnia[49].

Tfap2b is more widely expressed in the embryonic brain[50] and it may play a crucial role in the differentiation of sleep-promoting neurons. The mechanisms of sleep regulation by AP-2 transcription factors are best studied in nematodes, wherein the GABAergic neuron RIS plays a crucial role in the induction of sleep[19]. The nematode orthologue APTF-1 is selectively expressed in RIS, and APTF-1 exerts its sleep-promoting effect by promoting the transcription of the neuropeptide FLP-11 in RIS[19]. Thus, TFAP2B may contribute to mouse sleep regulation by promoting the transcription or synthesis of neuropeptides or other neuromodulators within sleep-promoting neurons.

The information on gene mutation, predicted human mRNA, mouse mRNA, mouse protein, and mouse sleep phenotypes are summarized in Fig. 21.

Human kindred 145 mRNA is predicted to result in the skipping of exon 5 because of

a single nucleotide mutation in the splice acceptor site just before exon 5. However, the RT-PCR and sequencing results of mice cDNA revealed that two mRNA products were formed, one lacking the first two nucleotides of exon 5 and the other lacking exon 5. In both cases, the variation in the mRNA sequence leads to a frameshift that generates a premature stop codon. The predicted protein size of the mRNA lacking exon 5 is 31 kDa, and that of the mRNA lacking the first two bases of exon 5 is 36 kDa, both smaller than the WT TFAP2B protein. However, no bands of these sizes were detected in the Western blotting, suggesting that scant or no proteins of such size were produced. Given that *Tfap2b*$^{K145/+}$ female mice show fragmentation in non-REM sleep, it is likely that the *Tfap2b*^{K145} mutation affects TFAP2B function in a manner different from that of *Tfap2b* KO.

The human kindred 144 mRNA has a single nucleotide mutation in the splice donor site immediately after exon 3, which purportedly results in the skipping of exon 3 based on the results of *in vitro* experiments[17]. The *Tfap2b*^{K144} mutations mimicked mutations identified in human kindred 144, but the cDNA sequence was unchanged in the case of mice. Since the protein size or expression level did not change, it is unlikely that this mutation affected the structure or overall expression of the TFAP2B protein. The mutation might have affected sleep by affecting the site of *Tfap2b* expression.

Tfap2b^{-} mice lack exon 3, and a poly-A transcription termination signal is inserted downstream of exon 2, thus likely resulting in termination of the transcription at exon 2. The predicted size of the protein formed by exon 1–2 is 20 kDa, but no such bands were observed on Western blotting. Non-REM sleep amount was reduced in female *Tfap2b*$^{+/-}$ mice and male *Nestin-Cre; Tfap2b*$^{flox/flox}$ mice, indicating that TFAP2B is involved in the regulation of non-REM sleep amount during nervous system development.

In summary, by generating *Tfap2b*^{K144} and *Tfap2b*^{K145} mutant mice and comparing their sleep with that of *Tfap2b*$^{+/-}$ mice, I revealed that *Tfap2b* is involved in the regulation of sleep in mice and that different mutations within *Tfap2b* have diverse effects on sleep. Moreover, I found that nervous system-specific *Tfap2b* deletion affects the sleep/wake cycle. This study demonstrates that TFAP2B is required for the

development of normal sleep patterns in mice and further supports the important and complicated roles of AP-2 transcription factors in sleep regulation.

Acknowledgments

I deeply thank my collaborators, Dr. Tomoyuki Fujiyama, Dr. Nanae Nagata, Dr. Mitsuaki Kashiwagi, Dr. Arisa Hirano, Ms. Aya Ikkyu, Ms. Marina Takagi, Ms. Chika Tatsuzawa, Ms. Kaeko Tanaka, Ms. Miyo Kakizaki, Ms. Ruoshi LI, Ms. Mika Kanuka, Dr. Taizo Kawano, Dr. Seiya Mizuno, Dr. Fumihiro Sugiyama, Dr. Satoru Takahashi, Dr. Hiromasa Funato, Dr. Takeshi Sakurai, Dr. Masashi Yanagisawa, and Dr. Yu Hayashi, for their kind support in conducting this study.

References

1. Miyazaki, S., Liu, C. Y. & Hayashi, Y. Sleep in vertebrate and invertebrate animals, and insights into the function and evolution of sleep. *Neuroscience Research* **118**, 3–12 (2017).
2. Campbell, S. S. & Tobler, I. Animal sleep: a review of sleep duration across phylogeny. *Neuroscience and biobehavioral reviews* **8**, 269–300 (1984).
3. Raizen, D. M. *et al.* Lethargus is a Caenorhabditis elegans sleep-like state. *Nature* **451**, 569–572 (2008).
4. Nelson, M. D. *et al.* FMRFamide-like FLP-13 Neuropeptides Promote Quiescence following Heat Stress in Caenorhabditis elegans. *Current Biology* **24**, 2406–2410 (2014).
5. Hill, A. J., Mansfield, R., Lopez, J. M. N. G., Raizen, D. M. & van Buskirk, C. Cellular stress induces a protective sleep-like state in C. elegans. *Current Biology* **24**, 2399–2405 (2014).
6. Konietzka, J. *et al.* Epidermal Growth Factor Signaling Promotes Sleep through a Combined Series and Parallel Neural Circuit. *Current Biology* **30**, 1–16.e13 (2020).
7. Shi, G., Wu, D., Ptáček, L. J. & Fu, Y. H. Human genetics and sleep behavior. *Current Opinion in Neurobiology* vol. **44**, 43–49 (2017).
8. He, Y. *et al.* The Transcriptional Repressor DEC2 Regulates Sleep Length in Mammals. *Science* **197**, 866–871 (2009).
9. Shi, G. *et al.* A Rare Mutation of β1-Adrenergic Receptor Affects Sleep/Wake Behaviors. *Neuron* 1–12 (2019).
10. Xing, L. *et al.* Mutant neuropeptide S receptor reduces sleep duration with preserved memory consolidation. *Science Translational Medicine* **11**, 1–12 (2019).
11. Shi, G. *et al.* Mutations in Metabotropic Glutamate Receptor 1 Contribute to Natural Short Sleep Trait. *Current Biology* **31**, 13-24.e4 (2021).
12. Sunagawa, G. A. *et al.* Mammalian Reverse Genetics without Crossing Reveals Nr3a as a Short-Sleeper Gene. *Cell Reports* **14**, 662–677 (2016).
13. Wisor, J. P. *et al.* Dopaminergic role in stimulant-induced wakefulness. *Journal of Neuroscience* **21**, 1787–1794 (2001).
14. Funato, H. *et al.* Forward-genetics analysis of sleep in randomly mutagenized mice. *Nature* **539**, 378–383 (2016).
15. Satoda, M. *et al.* Mutations in TFAP2B cause Char syndrome, a familial form of patent ductus arteriosus. *Nature Genetics* **25**, 42–46 (2000).

16. Davidson, H. R. A large family with patent ductus arteriosus and unusual face. *Journal of Medical Genetics* **30**, 503–505 (1993).
17. Mani, A. *et al.* Syndromic patent ductus arteriosus: Evidence for haploinsufficient TFAP2B mutations and identification of a linked sleep disorder. *Proceedings of the National Academy of Sciences of the United States of America* **102**, 2975–2979 (2005).
18. Castelnovo, A. *et al.* NREM sleep parasomnias as disorders of sleep-state dissociation. *Nature Reviews Neurology* 8 , 470-481 (2018).
19. Turek, M., Lewandrowski, I. & Bringmann, H. An AP2 transcription factor is required for a sleep-active neuron to induce sleep-like quiescence in C. elegans. *Current Biology* **23**, 2215–2223 (2013).
20. Turek, M., Besseling, J., Spies, J. P., König, S. & Bringmann, H. Sleep-active neuron specification and sleep induction require FLP-11 neuropeptides to systemically induce sleep. *eLife* **5**, 1–18 (2016).
21. Kucherenko, M. M., Ilangovan, V., Herzig, B., Shcherbata, H. R. & Bringmann, H. TfAP-2 is required for night sleep in Drosophila. *BMC Neuroscience* **17**, 1–11 (2016).
22. Williams, T. & Tjian, R. Characterization of a dimerization motif in AP-2 and its function in heterologous DNA-binding proteins. *Science* **251**, 1067–1071 (1991).
23. Eckert, D. Buhl, S. Weber, S. Jäger, R. & Schorle, H. The AP-2 family of transcription factors. *Genome Biology* **6**, 246 (2005).
24. Kim, H. S., Hong, S. J., Ledoux, M. S. & Kim, K. S. Regulation of the tyrosine hydroxylase and dopamine ß-hydroxylase genes by the transcription factor AP-2. *Journal of Neurochemistry* **76**, 280–294 (2001).
25. Moser, M. *et al.* Terminal renal failure in mice lacking transcription factor AP-2ß. *Laboratory Investigation* **83**, 571–578 (2003).
26. Moser, M. *et al.* Enhanced apoptotic cell death of renal epithelial cells in mice lacking transcription factor AP-2ß. *Genes and Development* **11**, 1938–1948 (1997).
27. Seki, R. *et al.* AP-2ß is a transcriptional regulator for determination of digit length in tetrapods. *Developmental Biology* **407**, 75–89 (2015).
28. Jin, K. *et al.* Tfap2a and 2b act downstream of Ptf1a to promote amacrine cell differentiation during retinogenesis. *Molecular Brain* **8**, 1–14 (2015).
29. Hicks, E. A. *et al.* Conditional deletion of AP-2α and AP-2ß in the developing murine retina leads to altered amacrine cell mosaics and disrupted visual function. *Investigative Ophthalmology and Visual Science* **59**, 2229–2239 (2018).

30. Seok, J. H. *et al.* Regulation of the noradrenaline neurotransmitter phenotype by the transcription factor AP-2ß. *Journal of Biological Chemistry* **283**, 16860–16867 (2008).
31. Schmidt, M. *et al.* The transcription factors AP-2ß and AP-2α are required for survival of sympathetic progenitors and differentiated sympathetic neurons. *Developmental Biology* **355**, 89–100 (2011).
32. Stocks, T. *et al.* TFAP2B influences the effect of dietary fat on weight loss under energy restriction. *PLoS ONE* **7**, (2012).
33. Martino, V. B. *et al.* Conditional deletion of AP-2ß in mouse cranial neural crest results in anterior segment dysgenesis and early-onset glaucoma. *DMM Disease Models and Mechanisms* **9**, 849–861 (2016).
34. Skarnes, W. C. *et al.* A conditional knockout resource for the genome-wide study of mouse gene function. *Nature* **474**, 337–344 (2011).
35. Niwa, H. *et al.* An efficient gene-trap method using poly a trap vectors and characterization of gene-trap events. *Journal of Biochemistry* **113**, 343–349 (1993).
36. Kanki, H., Suzuki, H. & Itohara, S. High-efficiency CAG-FLPe deleter mice in C57BL/6J background. *Experimental Animals* **55**, 137–141 (2006).
37. Isaka, F. *et al.* Ectopic expression of the bHLH gene Math1 disturbs neural development. *European Journal of Neuroscience* **11**, 2582–2588 (1999).
38. Neff, M. *et al.* dCAPS, a simple technique for the genetic analysis of single nucleotide polymorphisms: Experimental applications in Arabidopsis thaliana genetics. *Plant Journal* **14**, 387–392 (1998).
39. Hayashi, Y. *et al.* Cells of a common developmental origin regulate REM/non-REM sleep and wakefulness in mice. *Science* **350**, 957–961 (2015).
40. Honda, T. *et al.* A single phosphorylation site of SIK3 regulates daily sleep amounts and sleep need in mice. *Proceedings of the National Academy of Sciences of the United States of America* **115**, 10458–10463 (2018).
41. Koehl, M., Battle, S. & Meerlo, P. Sex differences in sleep: The response to sleep deprivation and restraint stress in mice. *Sleep* **29**, 1224–1231 (2006).
42. Koehl, M., Battle, S. & Turek, F. Sleep in female mice: A strain comparison across the estrous cycle. *Sleep* **26**, 267–272 (2003).
43. El-Brolosy, M. A. *et al.* Genetic compensation triggered by mutant mRNA degradation. *Nature* **568**, 193–197 (2019).
44. Miller, A. M., Obermeyer, W. H., Behan, M. & Benca, R. M. The superior colliculus-pretectum mediates the direct effects of light on sleep. *Proceedings of*

the National Academy of Sciences of the United States of America **95**, 8957–8962 (1998).

45. Aston-Jones, G. & Bloom, F. E. Activity of norepinephrine-containing locus coeruleus neurons in behaving rats anticipates fluctuations in the sleep-waking cycle. *Journal of Neuroscience* **1**, 876–886 (1981).
46. Carter, M. E. *et al.* Tuning arousal with optogenetic modulation of locus coeruleus neurons. *Nature Neuroscience* **13**, 1526–1535 (2010).
47. Yamaguchi, H., Hopf, F. W., Li, S. bin & de Lecea, L. In vivo cell type-specific CRISPR knockdown of dopamine beta hydroxylase reduces locus coeruleus evoked wakefulness. *Nature Communications* **9**, 1–8 (2018).
48. Fuller, P., Pederson, P., Saper, C. & Lu J. Reassessment of the structural basis of the ascending arousal system. *Journal of Comparative Neurology* **519**, 933–956 (2011).
49. Bonvallet, M. & Allen, M. B. Prolonged spontaneous and evoked reticular activation following discrete bulbar lesions. *Electroencephalography and Clinical Neurophysiology* **15**, 969–988 (1963).
50. Thompson, C. L. *et al.* A high-resolution spatiotemporal atlas of gene expression of the developing mouse brain. *Neuron* **83**, 309–323 (2014).

Figures

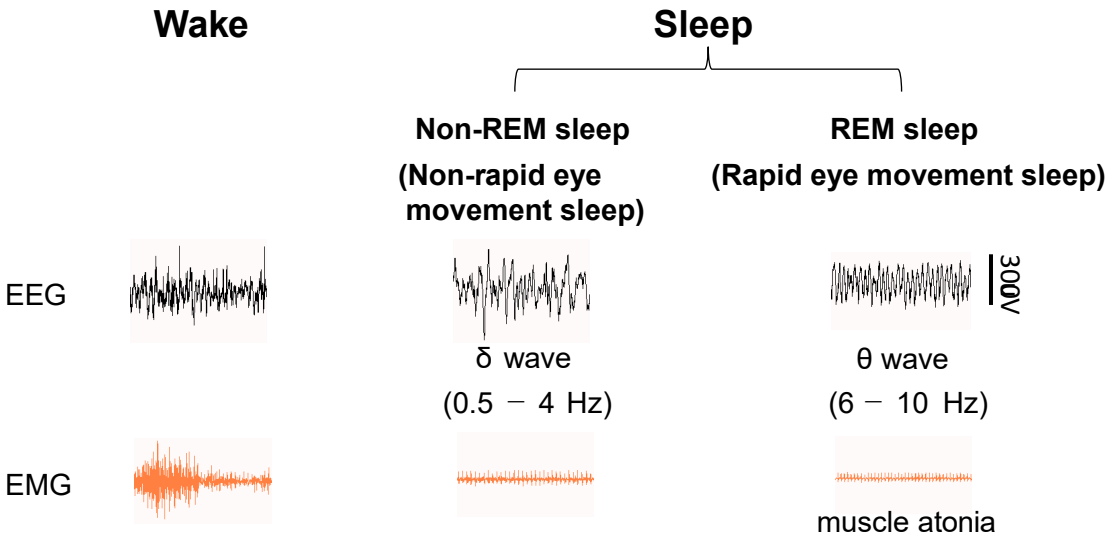

Fig. 1. Two sleep stages

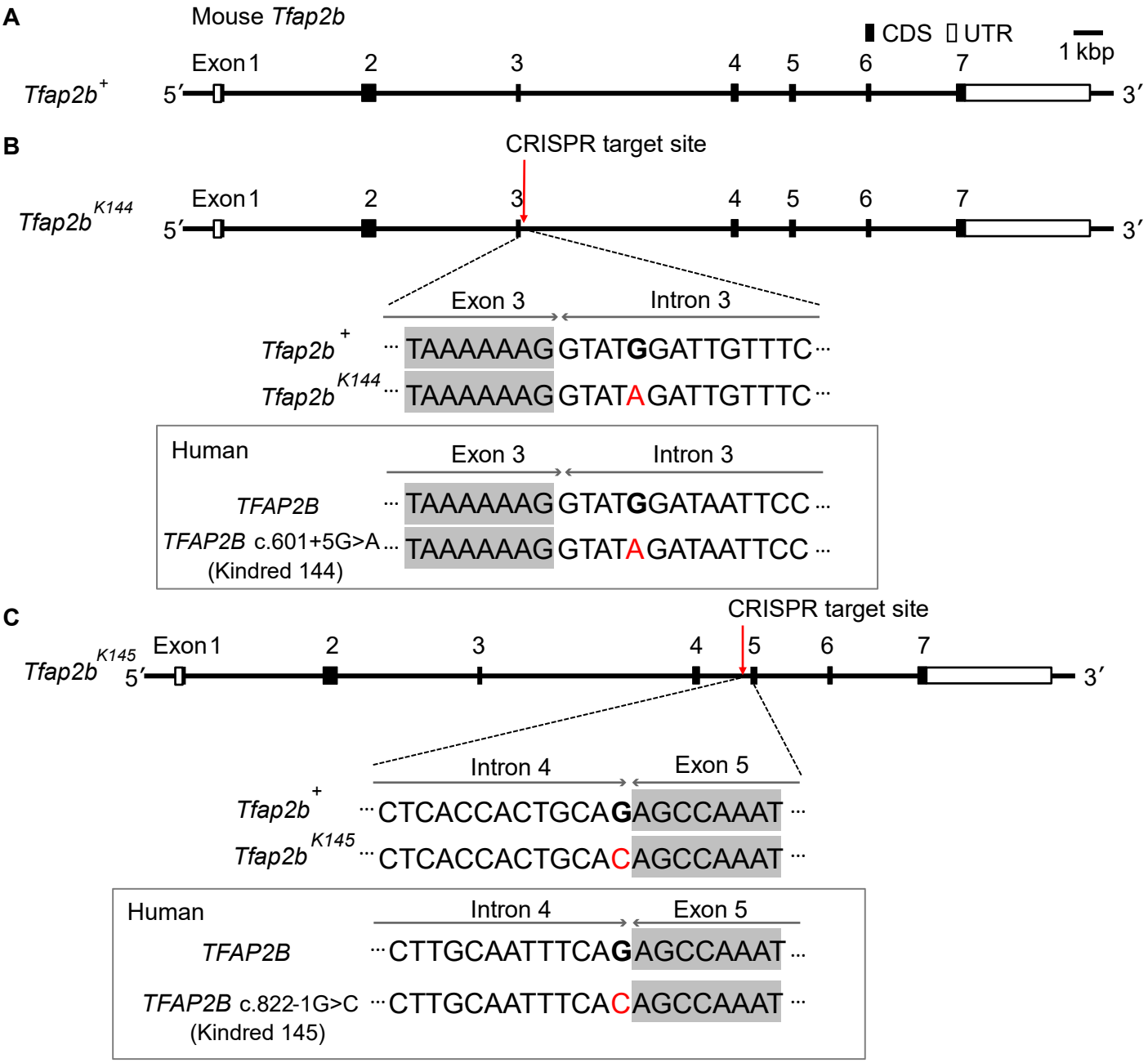

Fig. 2. Schematic diagram of the two mutant *Tfap2b* alleles, *Tfap2b*^{K144}, and *Tfap2b*^{K145} generated in this study

(A-C) Genomic structure around *Tfap2b* in WT (A), *Tfap2b*^{K144} (B), and *Tfap2b*^{K145} (C) and comparison of the DNA sequence around the mutation between mouse and human.

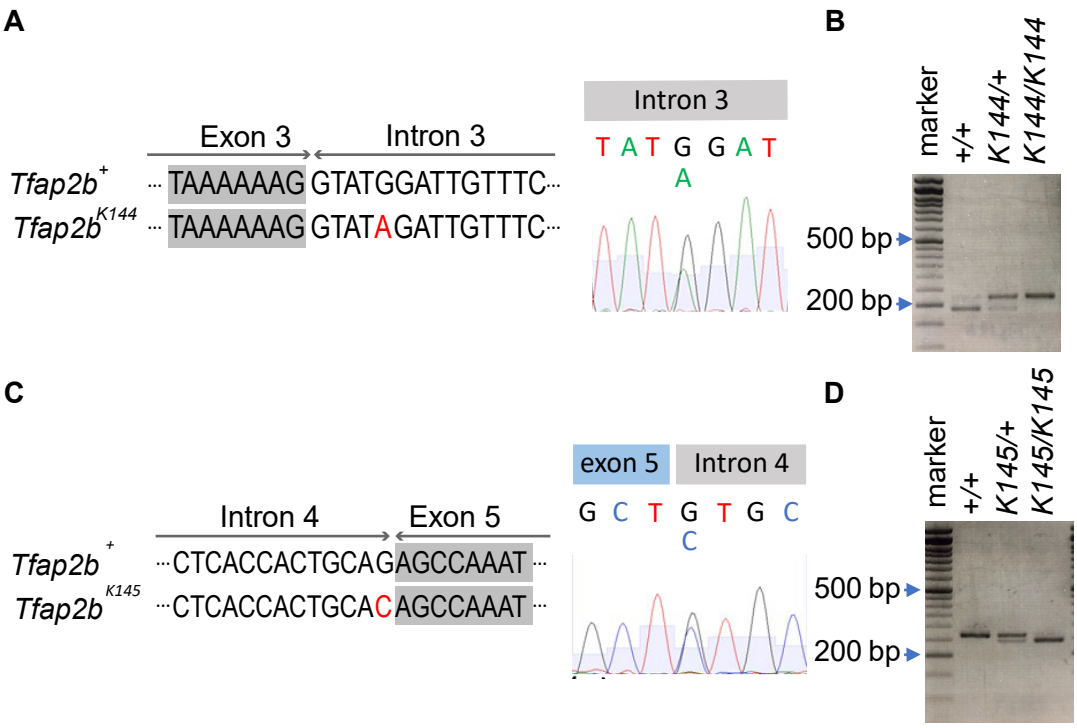

Fig. 3. Generation of *Tfap2b*^{K144} and *Tfap2b*^{K145} mutant mice

(A) Result of direct sequencing around the 5′ end of intron 3 in a *Tfap2b*$^{K144/+}$ mouse. (B) Results of dCAPS for genotyping of WT, *Tfap2b*$^{K144/+}$, and *Tfap2b*$^{K144/K144}$ mice. (C) Result of direct sequencing around the boundary of intron 4 and exon 5 in a *Tfap2b*$^{K145/+}$ mouse. Note that the results of sequencing of the anti-sense DNA strand is shown. (D) Results of dCAPS for genotyping of WT, *Tfap2b*$^{K145/+}$, and *Tfap2b*$^{K145/K145}$ mice.

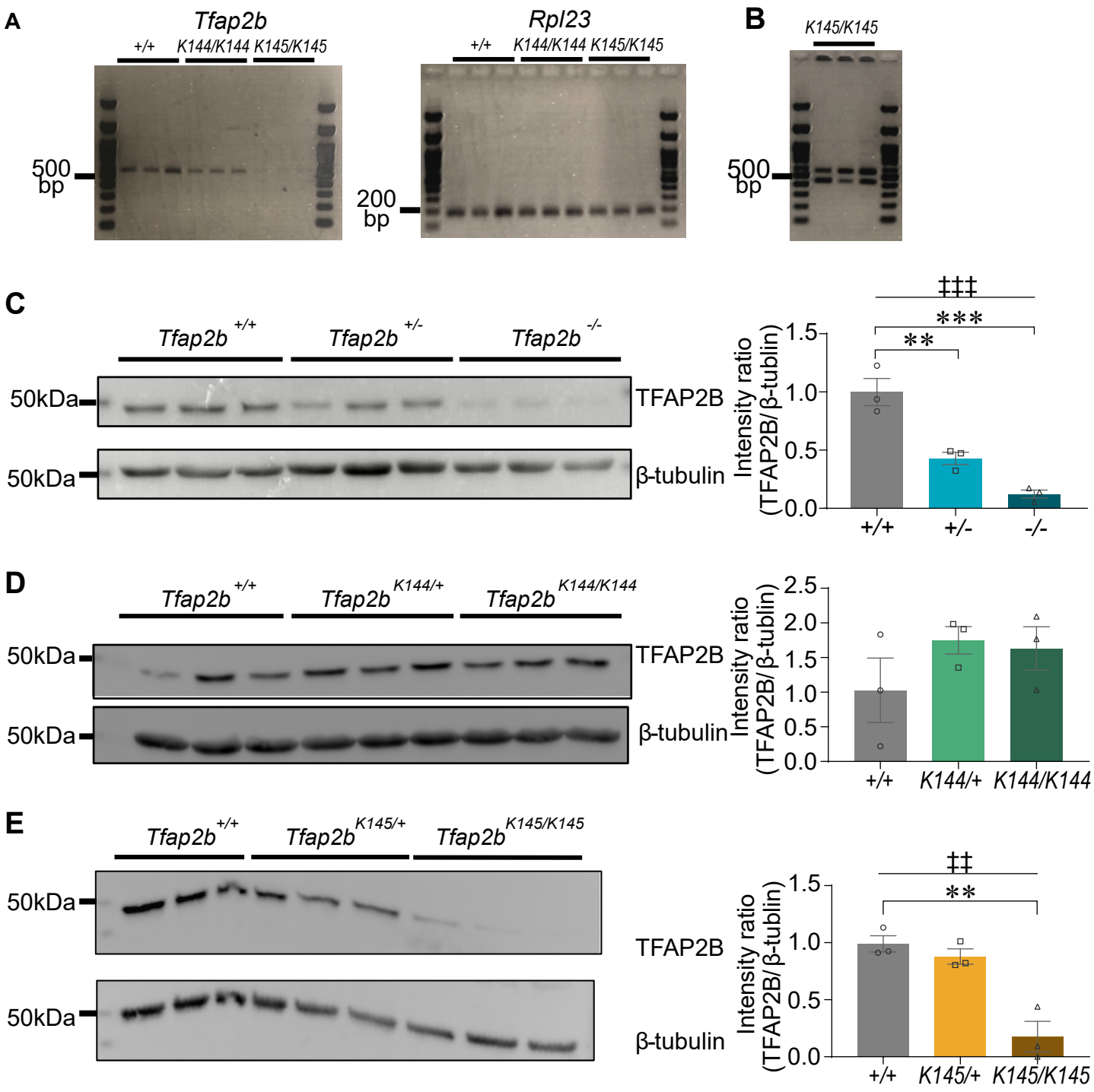

Fig. 4. RT-PCR and Western blot analyses of *Tfap2b* mutant mice

(A) Results of RT-PCR using total RNA from whole brain samples of *Tfap2b*$^{+/+}$, *Tfap2b*$^{K144/K144}$ and *Tfap2b*$^{K145/K145}$ mice at E18.5. For RT-PCR of *Tfap2b* mRNA, primers that flank exons 3–5 were used. (B) Increasing amplification cycles of *Tfap2b* RT–PCR in *Tfap2b*$^{K145/K145}$ mice resulted in two products of different size. Each lane represents an individual mouse. *N* = 3 mice. (C-E) Results of Western blot using an anti-TFAP2B antibody applied to whole brain samples from mice at E18.5 harboring *Tfap2b*$^{-}$ (C), *Tfap2b*^{K144} (D), or *Tfap2b*^{K145} (E). Each lane represents an individual mouse. *N* = 3 mice.
‡ indicates significance in one-way ANOVA (‡ ‡ $p < 0.01$, ‡ ‡ ‡ $p < 0.001$). * indicates significance in post-hoc Dunnet's test (** $p < 0.01$, *** $p < 0.001$). Data are presented as mean ± SEM.

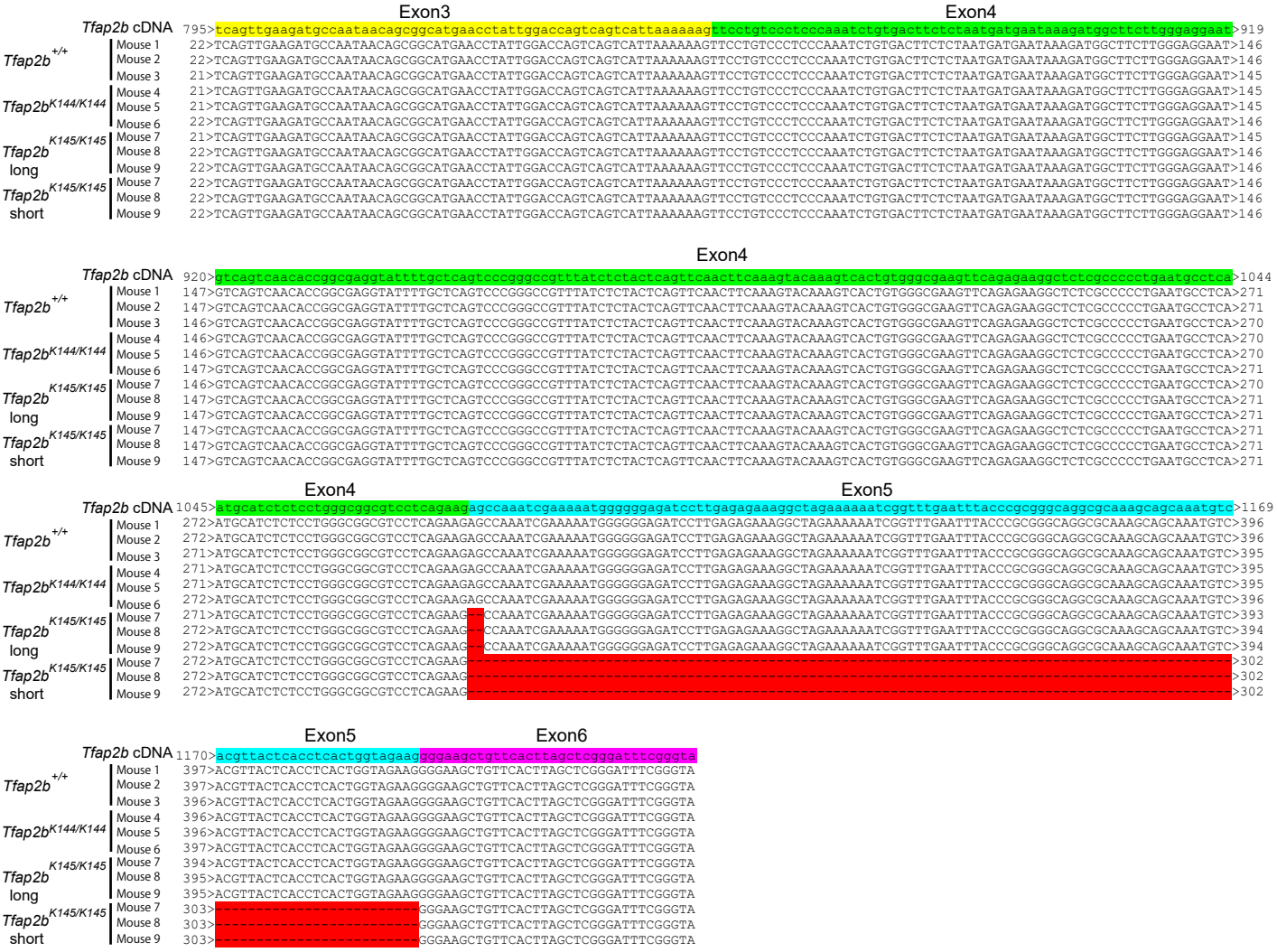

Fig. 5. Direct sequencing of *Tfap2b* mRNA in *Tfap2b* mutant mice

Nucleotide sequence alignment of *Tfap2b* mRNA around exon 3–6. Each lane represents an individual mouse. *N* = 3 mice.

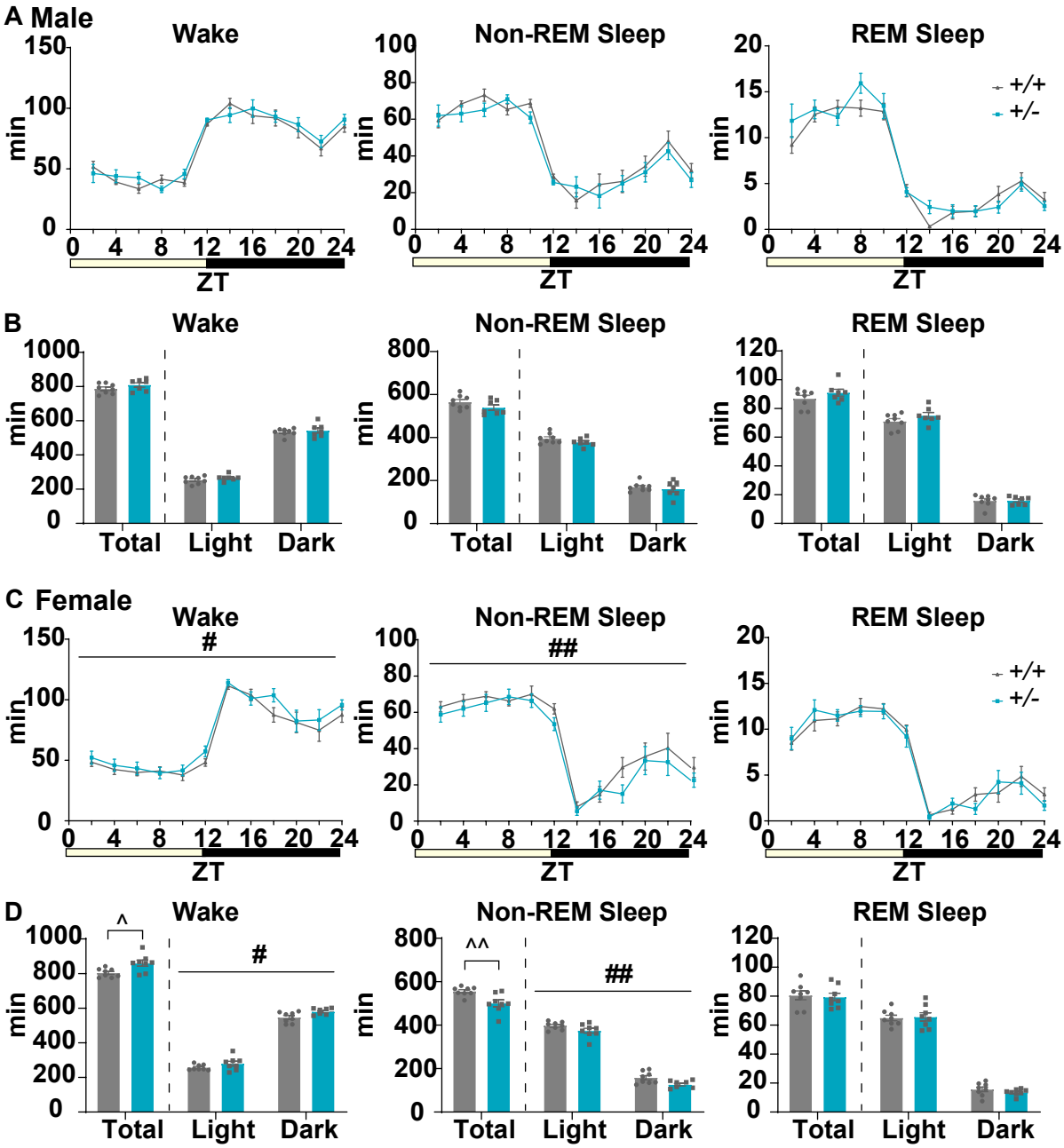

Fig. 6. Comparison of the amount of sleep/wake in adult *Tfap2b*$^{+/+}$ and *Tfap2b*$^{+/-}$ mice

(A) Bi-hourly amount of wakefulness, non-REM sleep, and REM sleep across 24 h in male mice. (B) Total amount of wakefulness, non-REM sleep, and REM sleep during 24 h, light phase, and dark phase in male mice. N = 8 *Tfap2b*$^{+/+}$ mice, N = 7 *Tfap2b*$^{+/-}$ mice. (C) Bi-hourly amount of wakefulness, non-REM sleep, and REM sleep across 24 h in female mice. (D) Total amount of wakefulness, non-REM sleep, and REM sleep during 24 h, light phase, and dark phase in female mice. N = 8 *Tfap2b*$^{+/+}$ mice, N = 8 *Tfap2b*$^{+/-}$ mice. # indicates significant main effect of genotype in two-way repeated-measures ANOVA (#$p < 0.05$, ##$p < 0.01$). ^ indicates significance in the Welch's test (^$p < 0.05$, ^^$p < 0.01$). Data are presented as mean ± SEM.

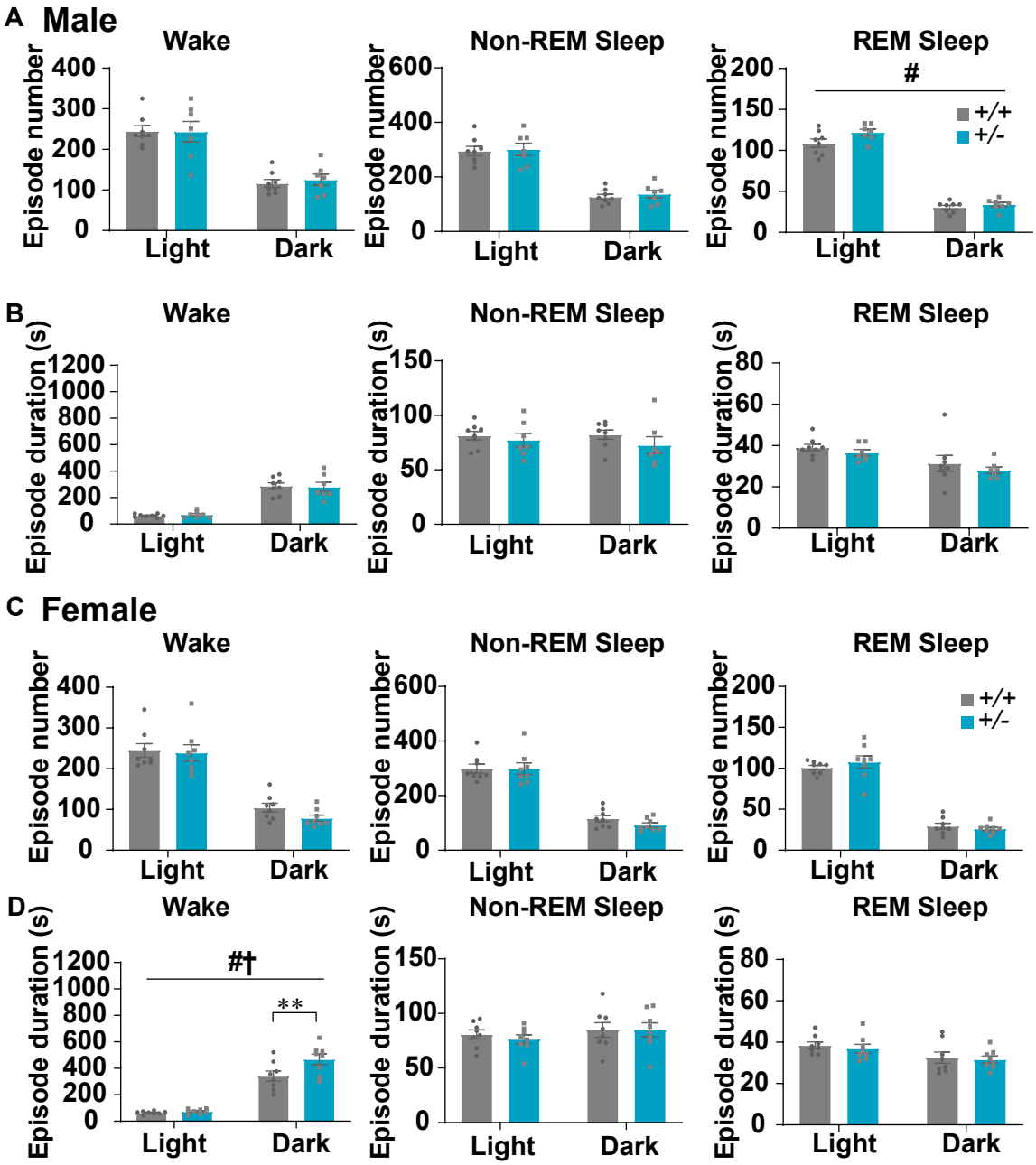

Fig. 7. Comparison of the numbers and durations of sleep/wake episodes in adult *Tfap2b*$^{+/+}$ and *Tfap2b*$^{+/-}$ mice

(A, B) Episode numbers (A) and durations (B) of wakefulness, non-REM sleep, and REM sleep during 24 h, light phase, and dark phase in male mice. *N* = 8 *Tfap2b*$^{+/+}$ mice, *N* = 7 *Tfap2b*$^{+/-}$ mice. (C, D) Episode numbers (C) and durations (D) of wakefulness, non-REM sleep, and REM sleep during 24 h, light phase, and dark phase in female mice. *N* = 8 *Tfap2b*$^{+/+}$ mice, *N* = 8 *Tfap2b*$^{+/-}$ mice. # and † indicate significant main effect of genotype and significant interaction between genotype and light/dark phase, respectively, in two-way repeated-measures ANOVA (#, † $p < 0.05$). * indicates significance in post-hoc Bonferroni multiple comparison test (** $p < 0.01$). Data are presented as mean ± SEM.

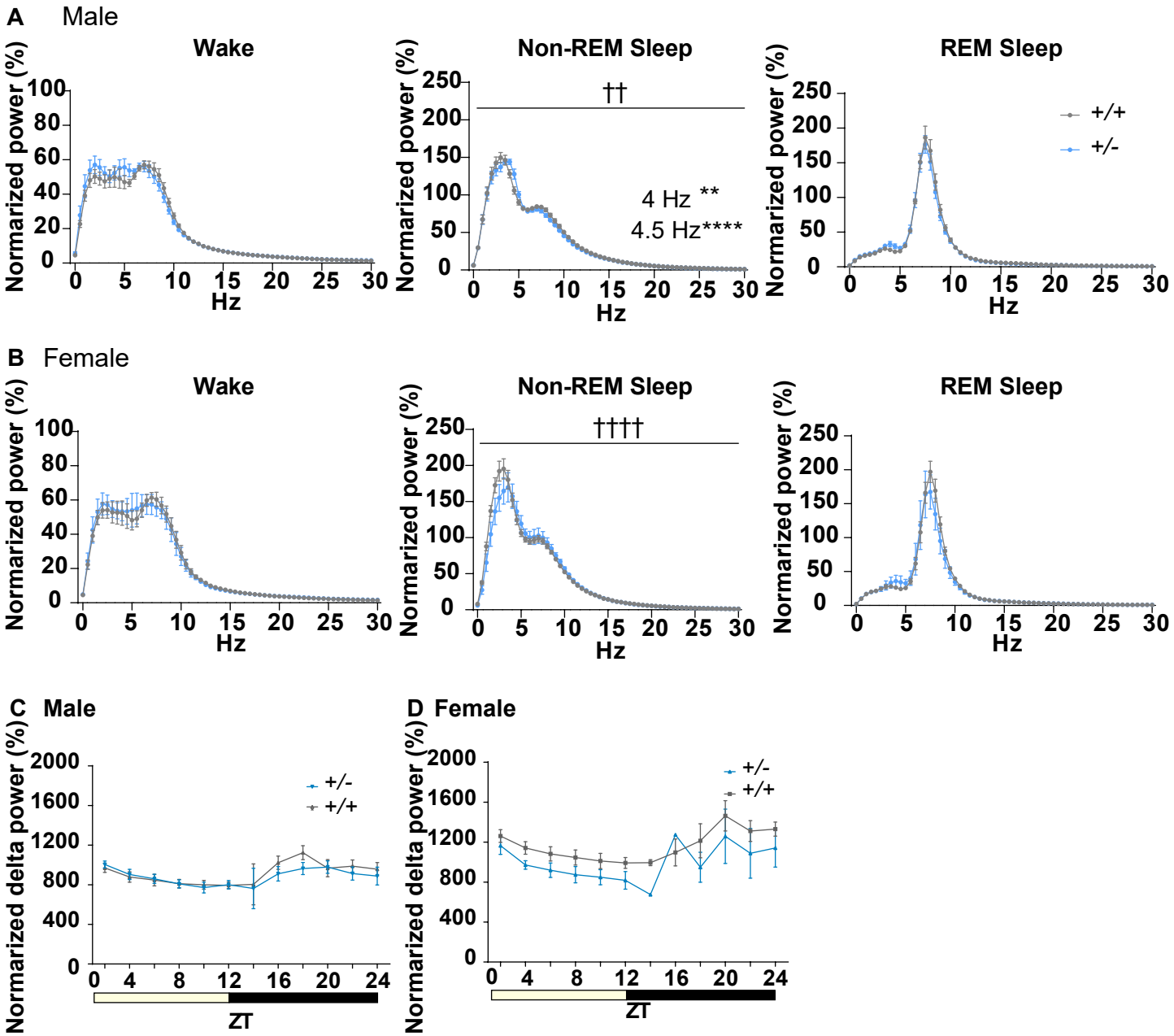

Fig. 8. Comparison of EEG power spectra and non-REM sleep delta density in adult *Tfap2b*$^{+/+}$ and *Tfap2b*$^{+/-}$ mice

(A, B) Comparison of the EEG power spectrum of wakefulness, non-REM sleep, and REM sleep for 24 h between male (A) or female (B). (C, D) Comparison of bi-hourly changes in non-REM sleep delta density between male (C) or female (D). *Tfap2b*$^{+/+}$ and *Tfap2b*$^{+/-}$ mice. N = 7 *Tfap2b*$^{+/+}$ male mice, N = 5 *Tfap2b*$^{+/-}$ male mice, N = 5 *Tfap2b*$^{+/+}$ female mice, N = 3 *Tfap2b*$^{+/-}$ female mice. † indicates significant interaction between frequency and genotype in two-way repeated- measures ANOVA († † p < 0.01; † † † † p < 0.0001). * indicates significance in post-hoc Bonferroni multiple comparison test (**p < 0.01, ****p < 0.0001). Data are presented as mean ± SEM.

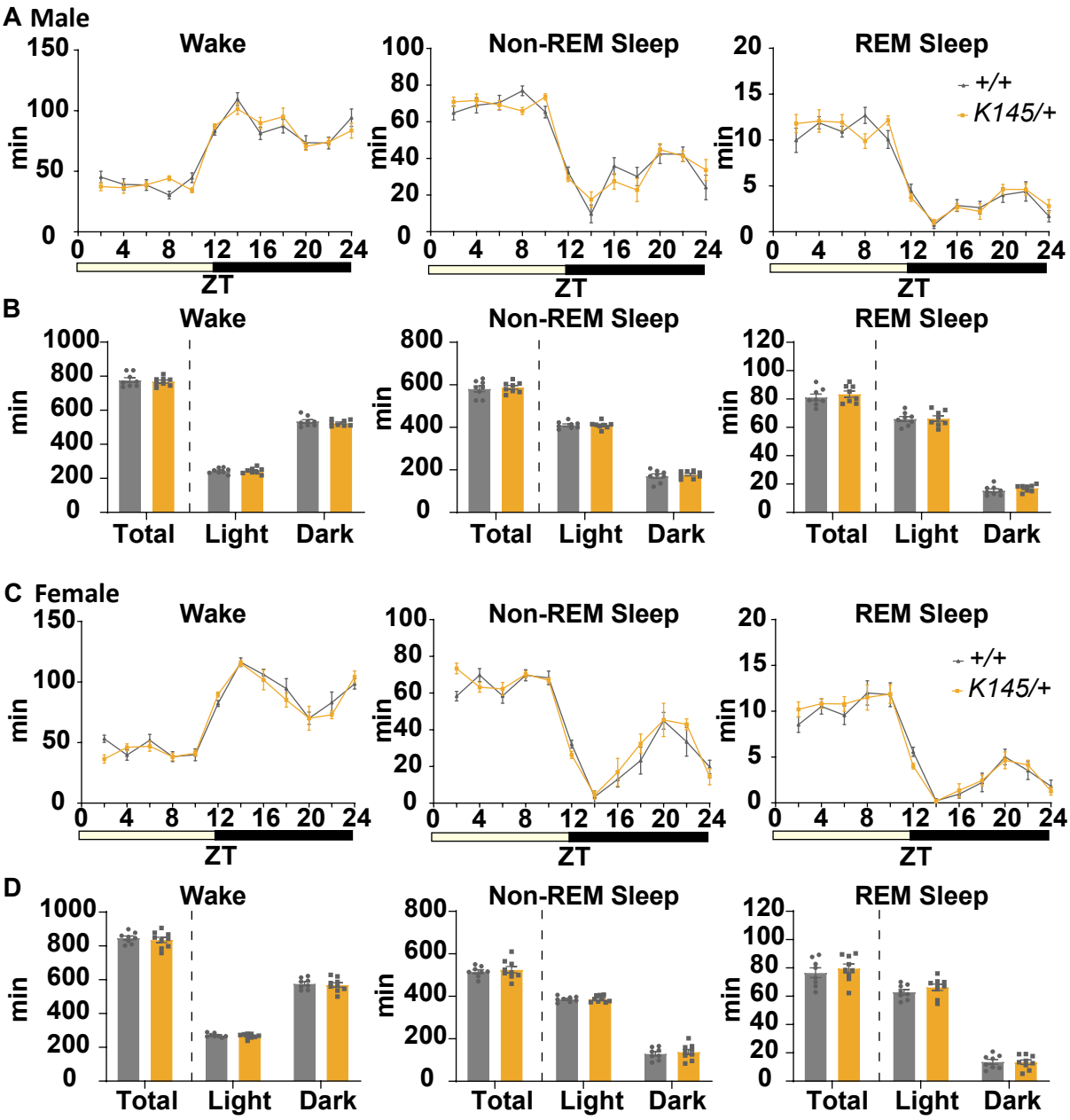

Fig. 9. Comparison of the amount of sleep/wake in adult *Tfap2b*$^{+/+}$ and *Tfap2b*$^{K145/+}$ mice

(A) Bi-hourly amount of wakefulness, non-REM sleep, and REM sleep across 24 h in male mice. (B) Total amount of wakefulness, non-REM sleep, and REM sleep during 24 h, light phase, and dark phase in male mice. *N* = 8 *Tfap2b*$^{+/+}$ mice, *N* = 8 *Tfap2b*$^{K145/+}$ mice. (C) Bi-hourly amount of wakefulness, non-REM sleep, and REM sleep across 24 h in female mice. (D) Total amount of wakefulness, non-REM sleep, and REM sleep during 24 h, light phase, and dark phase in female mice. *N* = 8 *Tfap2b*$^{+/+}$ mice, *N* = 9 *Tfap2b*$^{K145/+}$ mice. Data are presented as mean ± SEM.

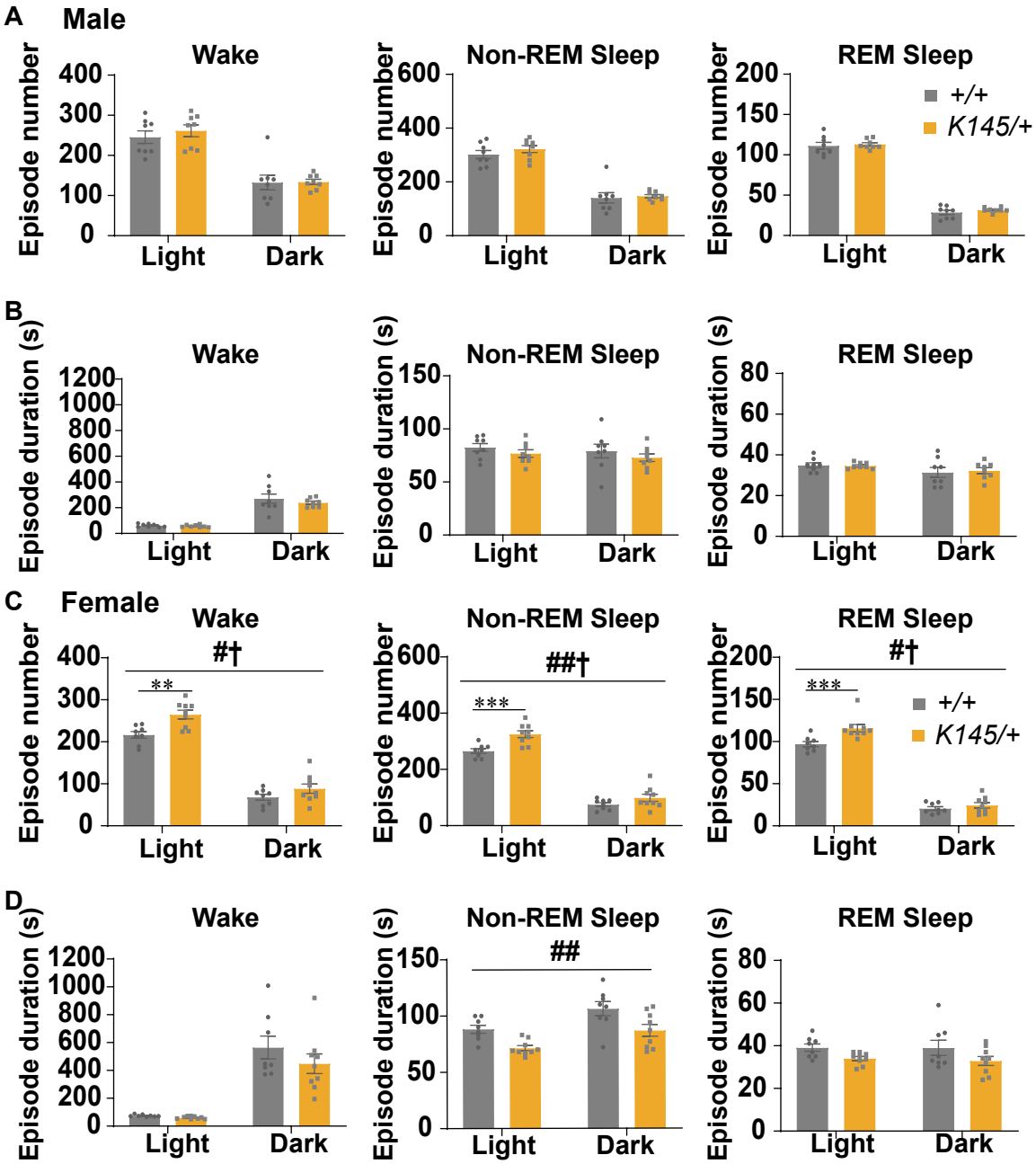

Fig. 10. Comparison of the sleep episode number and duration in adult *Tfap2b*$^{+/+}$ and *Tfap2b*$^{K145/+}$ mice

(A, B) Episode numbers (A) and durations (B) of wakefulness, non-REM sleep, and REM sleep during 24 h, light phase, and dark phase in male mice. *N* = 8 *Tfap2b*$^{+/+}$ mice, *N* = 8 *Tfap2b*$^{K145/+}$ mice. (C, D) Episode numbers (C) and durations (D) of wakefulness, non-REM sleep, and REM sleep during 24 h, light phase, and dark phase in female mice. *N* = 8 *Tfap2b*$^{+/+}$ mice, *N* = 9 *Tfap2b*$^{K145/+}$ mice. # and † indicate significant main effect of genotype and significant interaction between genotype and light/dark phase, respectively, in two-way repeated-measures ANOVA (#, † $p < 0.05$, ##$p < 0.01$). * indicates significance in post-hoc Bonferroni multiple comparison test (**$p < 0.01$, ***$p < 0.001$). Data are presented as mean ± SEM.

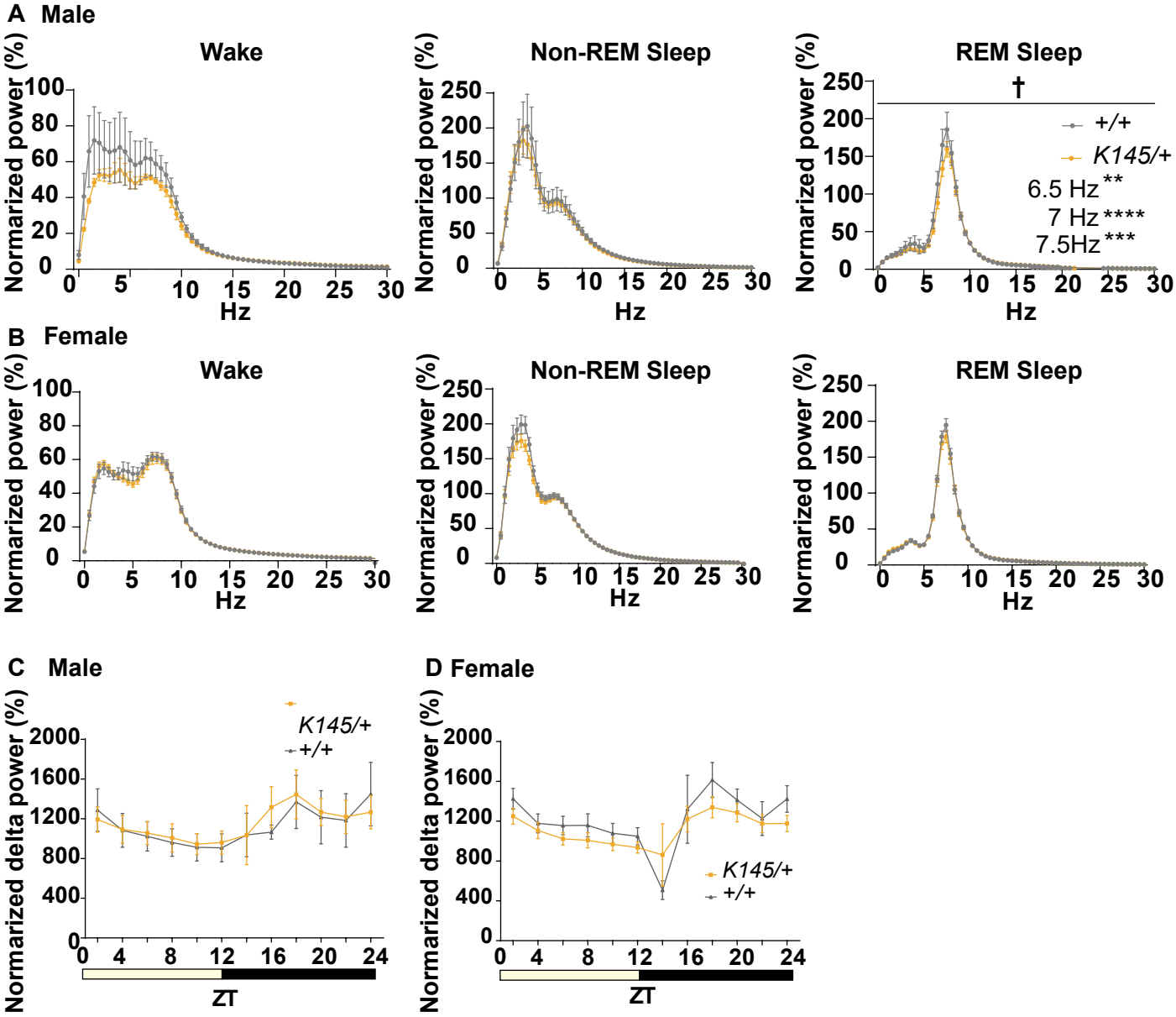

Fig. 11. Comparison of EEG power spectra and non-REM sleep delta density in adult *Tfap2b*$^{+/+}$ and *Tfap2b*$^{K145/+}$ mice

(A, B) Comparison of the EEG power spectrum of wakefulness, non-REM sleep, and REM sleep for 24 h between male (A) or female (B). (C, D) Comparison of bi-hourly changes in non-REM sleep delta density between male (C) or female (D). *Tfap2b*$^{+/+}$ and *Tfap2b*$^{K145/+}$ mice. N = 5 *Tfap2b*$^{+/+}$ male mice, N = 7 *Tfap2b*$^{K145/+}$ male mice, N = 8 *Tfap2b*$^{+/+}$ female mice, N = 9 *Tfap2b*$^{K145/+}$ female mice. † indicates significant interaction between frequency and genotype in two-way repeated- measures ANOVA († $p < 0.05$). * indicates significance in post-hoc Bonferroni multiple comparison test (**$p < 0.01$, ***$p < 0.001$, ****$p < 0.0001$). Data are presented as mean ± SEM.

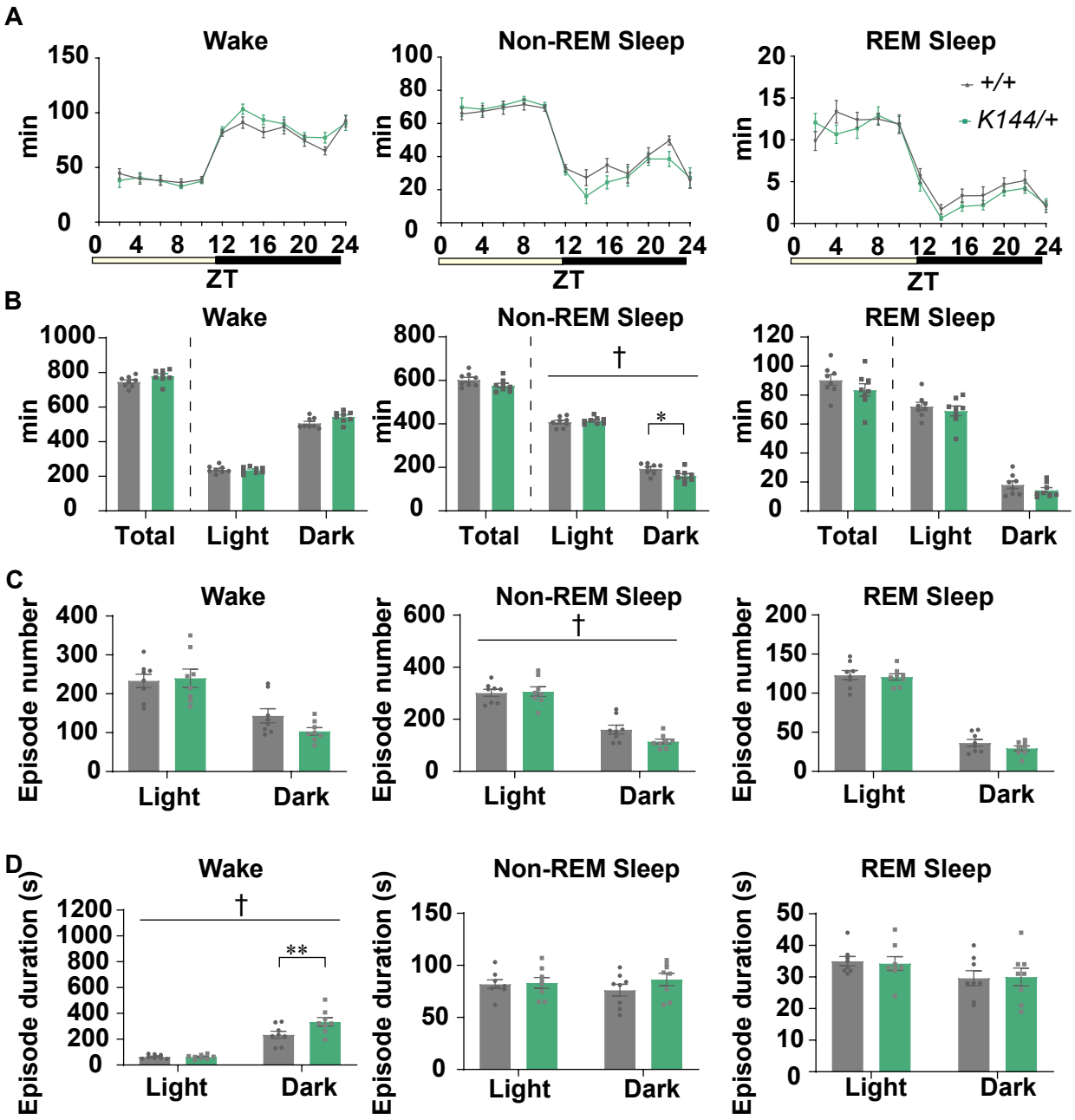

Fig. 12. Comparison of the sleep architecture in adult *Tfap2b*$^{+/+}$ and *Tfap2b*$^{K144/+}$ mice

(A) Bi-hourly amount of wakefulness, non-REM sleep, and REM sleep across 24 h in male mice. (B) Total amount of wakefulness, non-REM sleep, and REM sleep during 24 h, light phase, and dark phase in male mice. (C, D) Episode durations (C) and numbers (D) of wakefulness, non-REM sleep, REM sleep during 24 h, light phase, and dark phase in male mice. N = 8 *Tfap2b*$^{+/+}$ mice, N = 8 *Tfap2b*$^{K144/+}$ mice. † indicates significant interaction between genotype and Zeitgeber time (ZT) or light/dark phase in two-way repeated-measures ANOVA († p <0.05). * indicates significance in post-hoc Bonferroni multiple comparison test (*p < 0.05, **p < 0.01). Data are presented as mean ± SEM.

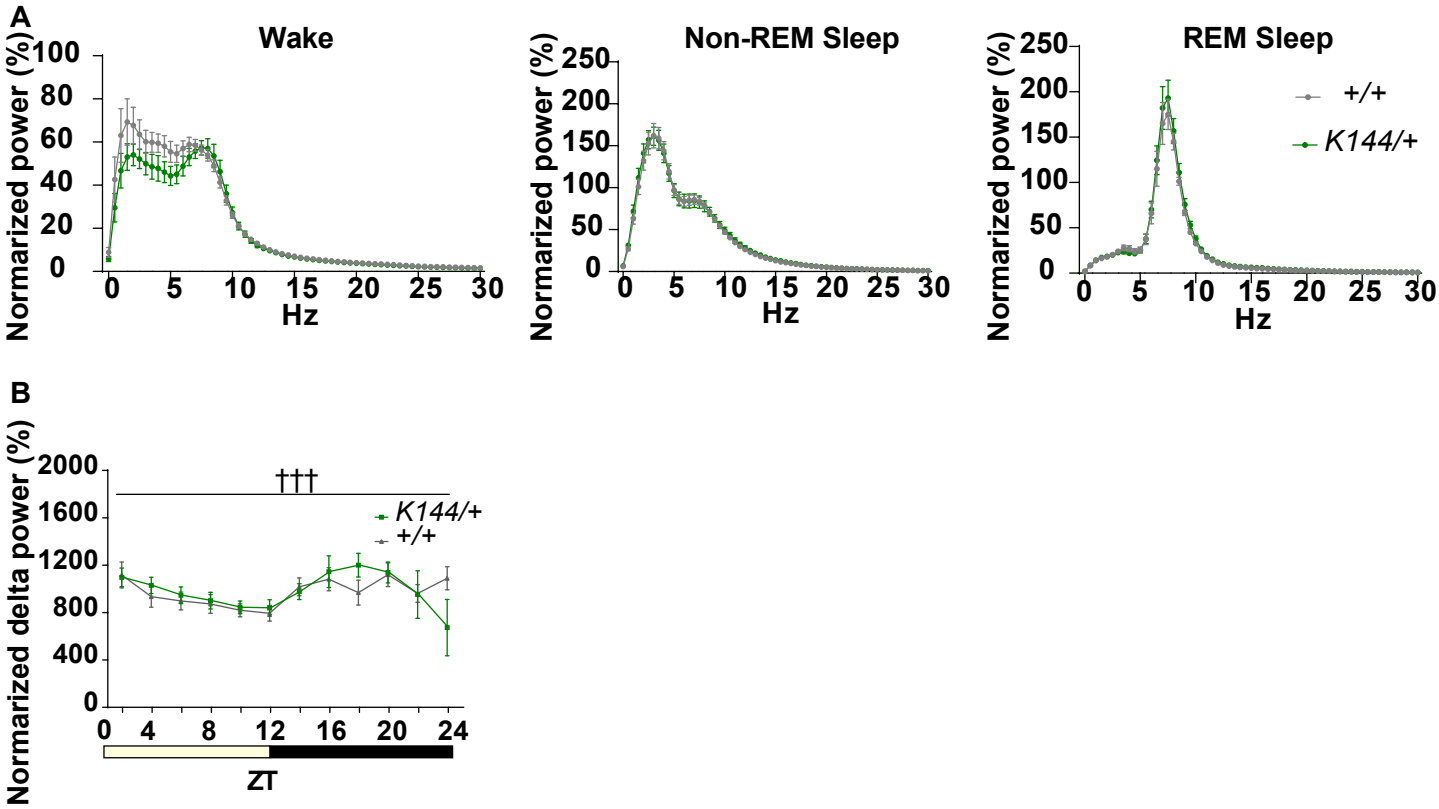

Fig. 13. Comparison of EEG power spectra and non-REM sleep delta density in adult *Tfap2b*$^{+/+}$ and *Tfap2b*$^{K144/+}$ male mice

(A, B) Comparison of the EEG power spectrum of wakefulness, non-REM sleep, and REM sleep for 24 h (A) and comparison of bi-hourly changes in non-REM sleep delta density (B) between male *Tfap2b*$^{+/+}$ and *Tfap2b*$^{K144/+}$ mice. *N* = 7 *Tfap2b*$^{+/+}$ male mice, *N* = 4 *Tfap2b*$^{K144/+}$ male mice. Data are presented as mean ± SEM.

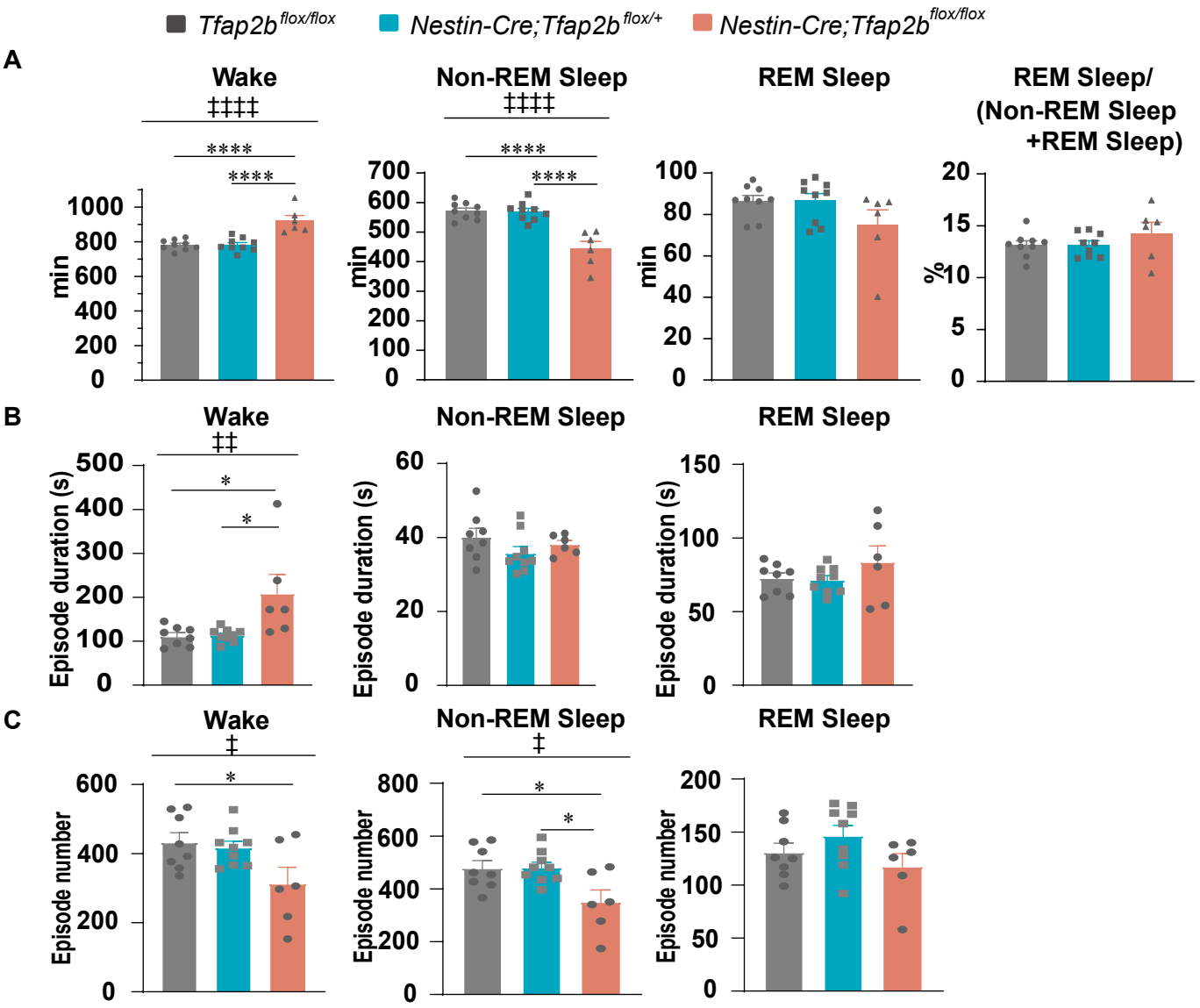

Fig. 14. Comparison of the sleep architecture in nervous system-specific *Tfap2b* cKO and control mice

(A) Total amount of wakefulness, non-REM sleep, REM sleep and REM sleep ratio per total sleep time during 24 h in male mice. $N = 9$ *Tfap2b*$^{flox/flox}$ mice, $N = 9$ *Nestin-Cre;Tfap2b*$^{flox/+}$ mice, $N = 6$ *Nestin-Cre;Tfap2b*$^{flox/flox}$ (B, C) Episode durations (B) and numbers (C) of wakefulness, non-REM sleep, REM sleep during 24 h in male mice. $N = 8$ *Tfap2b*$^{flox/flox}$ mice, $N = 9$ *Nestin-Cre;Tfap2b*$^{flox/+}$ mice, $N = 6$ *Nestin-Cre;Tfap2b*$^{flox/flox}$ ‡ indicates significance in one-way ANOVA (‡ $p < 0.05$, ‡‡ $p < 0.01$, ‡‡‡‡ $p < 0.0001$). * indicates significance in post-hoc Bonferroni multiple comparison test (*$p < 0.05$, ****$p < 0.0001$). Data are presented as mean ± SEM.

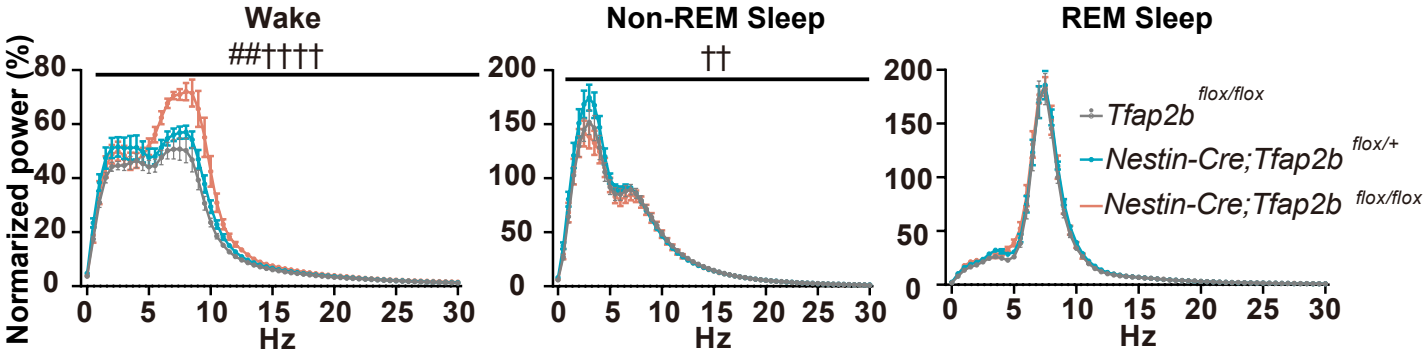

Wake post hoc test
Tfap2b$^{flox/flox}$ *vs Nestin-Cre;Tfap2b*$^{flox/+}$ 0.5 Hz
Tfap2b$^{flox/flox}$ *vs Nestin-Cre;Tfap2b*$^{flox/flox}$ 5.5, 8.5, 9.0, 10.5, 11.0, 15.5-17.0 Hz*, 6.0-8.0,11.5-15.0 Hz**,
Nestin-Cre;Tfap2b$^{flox/+}$ *vs Nestin-Cre;Tfap2b*$^{flox/flox}$ 6.0, 8.0, 13.0,13.5 Hz*, 6.5, 7.5 Hz**, 7.0 Hz***

Fig. 15. Comparison of EEG power spectra in nervous system-specific *Tfap2b* cKO and control mice

Comparison of the EEG power spectrum of wakefulness, non-REM sleep, and REM sleep for 24 h between *Tfap2b*$^{flox/flox}$, *Nestin-Cre;Tfap2b*$^{flox/+}$ and *Nestin-Cre;Tfap2b*$^{flox/flox}$ male mice. *N* = 8 *Tfap2b*$^{flox/flox}$ mice, *N* = 9 *Nestin-Cre;Tfap2b*$^{flox/+}$ mice and *N* = 6 *Nestin-Cre;Tfap2b*$^{flox/flox}$. # and † indicate significant main effect of genotype and significant interaction between frequency and genotype, respectively, in two-way repeated-measures ANOVA (##, † † $p < 0.01$, † † † † $p < 0.0001$), * indicates significance in post-hoc Bonferroni multiple comparison test (*$p < 0.05$, **$p < 0.01$, ***$p < 0.001$). Data are presented as mean ± SEM.

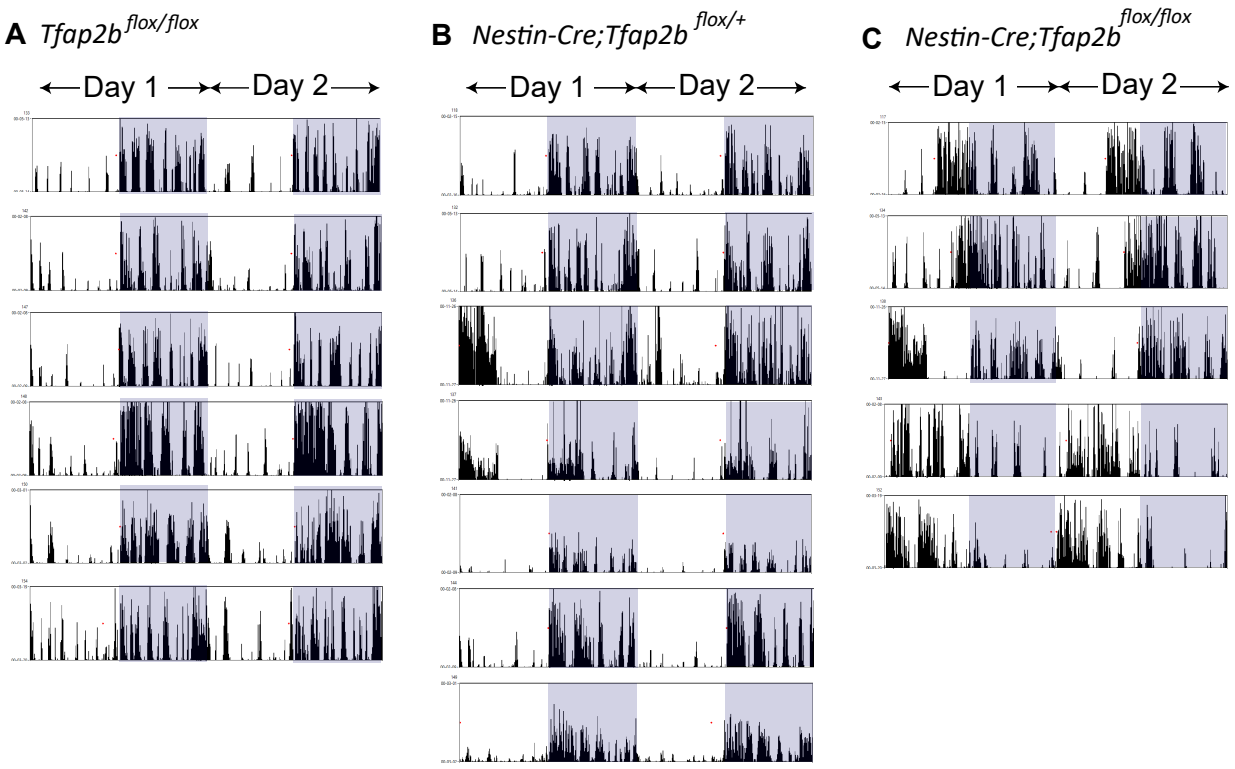

Fig. 16. Individual activity change of nervous system-specific *Tfap2b* KO and WT mice

(A-C) 2 days (5 min bin) infrared detected activity change of individual *Tfap2b*$^{flox/flox}$ mice (A), *Nestin-Cre;Tfap2b*$^{flox/+}$ mice (B), and *Nestin-Cre;Tfap2b*$^{flox/flox}$ mice (C).

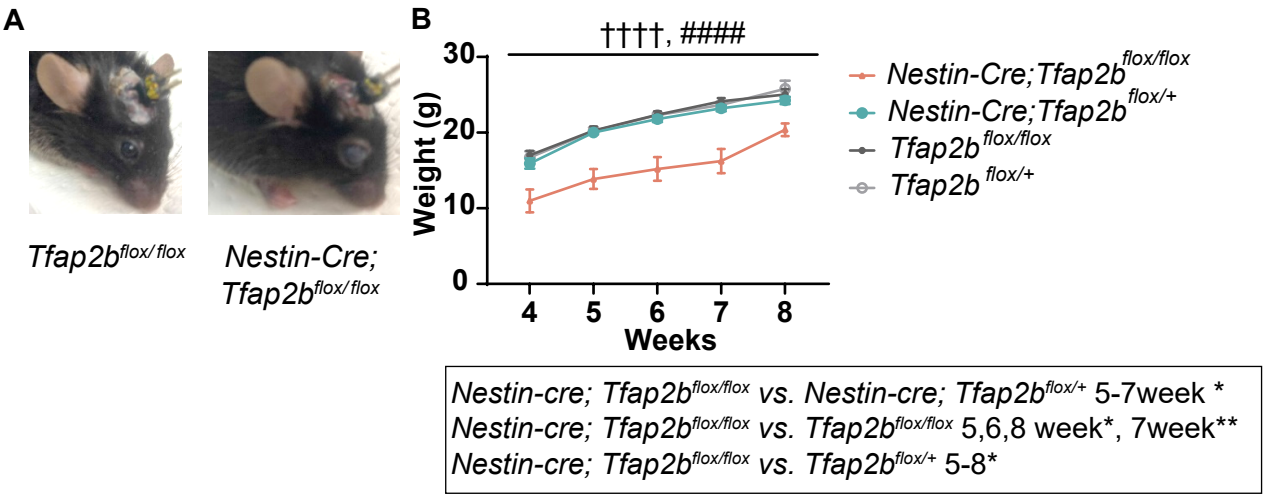

Fig. 17. Eye feature and bodyweight change of nervous system-specific Tfap2b cKO and control mice

(A) Image of *Tfap2b*$^{flox/flox}$ and *Nestin-Cre;Tfap2b*$^{flox/flox}$ mouse eye (B) Bodyweight change of nervous system-specific *Tfap2b* KO and WT mice. # and † indicate a significant main effect of genotype and significant interaction between genotype and weeks, respectively, in two-way repeated-measures ANOVA (####,††††p < 0.0001). * indicates significance in post-hoc Bonferroni multiple comparison test (*p < 0.05, **p < 0.01). Data are presented as mean ± SEM.

A *Tfap2b*$^{flox/flox}$

Actogram

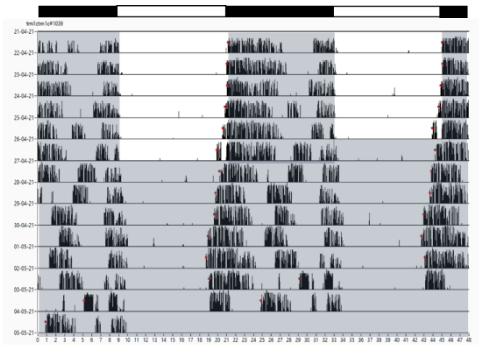

B *Nestin-Cre;Tfap2b*$^{flox/+}$

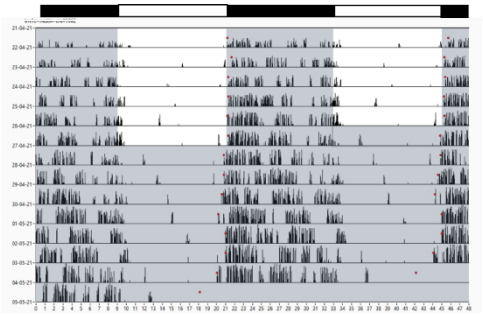

C *Nestin-Cre;Tfap2b*$^{flox/flox}$

#1

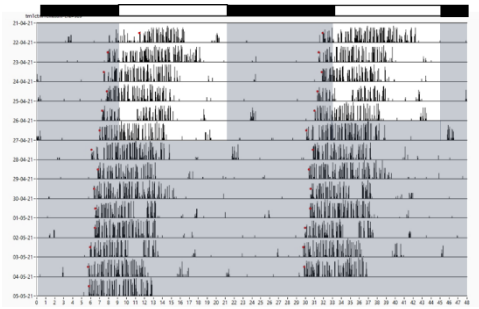

#2

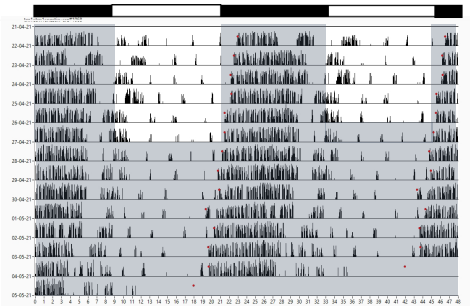

Fig. 18. Wheel running activity of nervous system-specific *Tfap2b* KO and WT mice

(A-C) Representative actograms of the wheel-running activities of *Tfap2b*$^{flox/flox}$ mice (A), *Nestin-Cre;Tfap2b*$^{flox/+}$ mice (B), and *Nestin-Cre;Tfap2b*$^{flox/flox}$ mice (C). Mice were entrained to LD cycle for at least 1 week, transferred to DD.

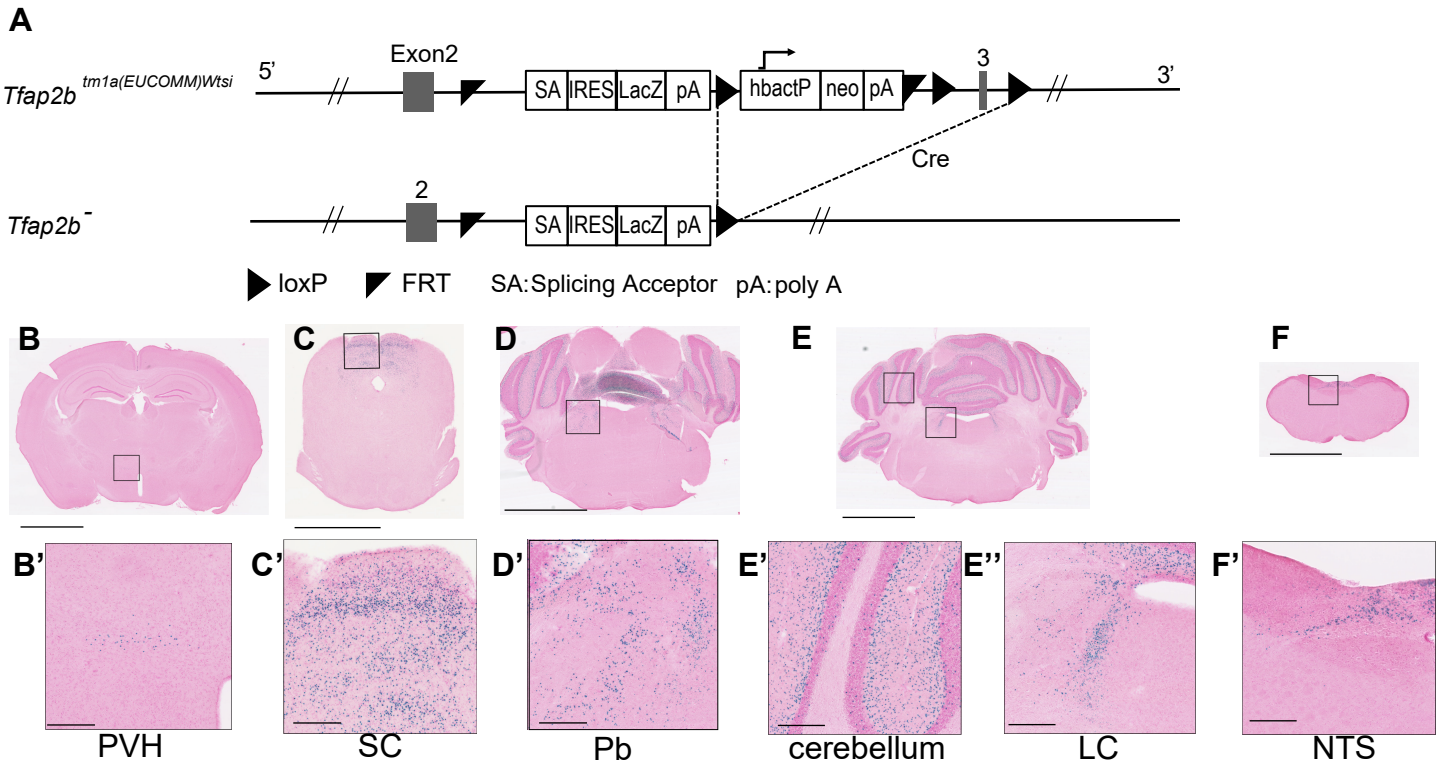

Fig. 19. Expression analyses of *Tfap2b* in the adult brain by X-gal staining of *Tfap2b*$^{+/-}$ mice

(A) Schematic diagram of the *Tfap2b*$^{-}$ allele used in this study. (B-F) Images of areas where LacZ-derived signals were detected. PVH, paraventricular hypothalamic nucleus (B'); SC, superior colliculus (C'); Pb, parabrachial nucleus (D'), cerebellum (E'), LC, locus coeruleus (E''); NTS, solitary tract nucleus (F'). Scale bars in (B-F), 2.5 mm; scale bars in (B'-E'), 250 μm. Representative images from a replicate of three mice are shown.

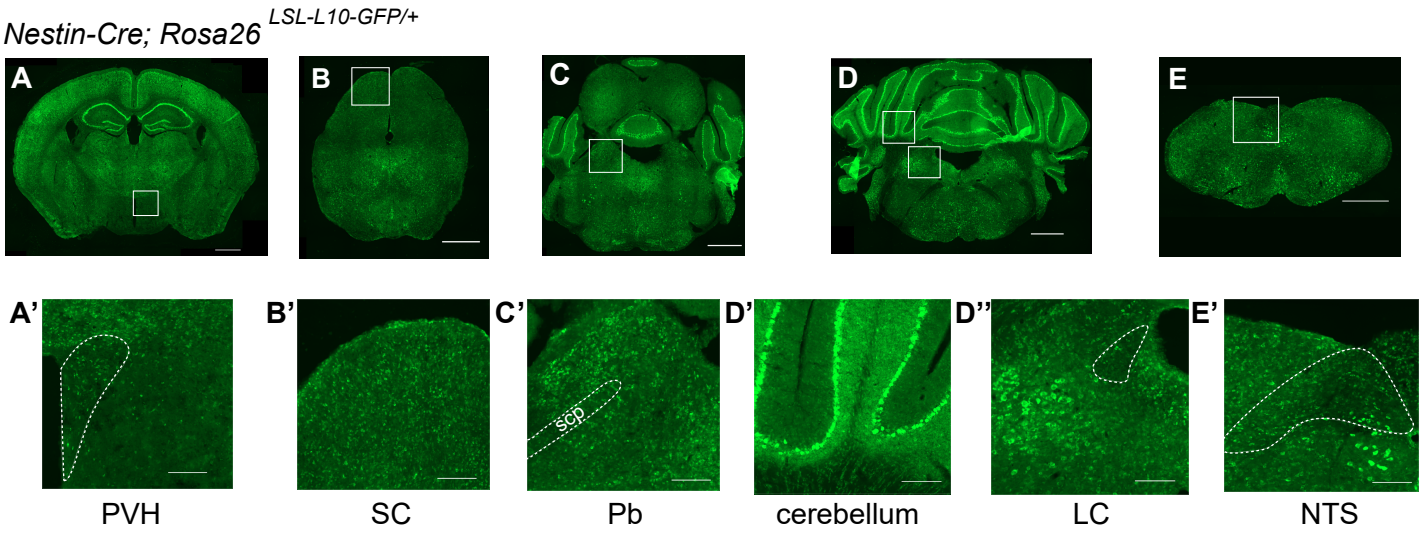

Fig. 20. Comparison of the Cre-mediated recombination patterns in *Nestin-Cre*

(A-E) Images of areas where GFP signals were detected from *Nestin-Cre; Rosa26* $^{LSL\text{-}L10\text{-}GFP/+}$ mice. PVH, paraventricular hypothalamic nucleus (A'); SC, superior colliculus (B'); Pb, parabrachial nucleus (C'); LC, locus coeruleus (D''); NTS, solitary tract nucleus (E'). scp, superior cerebellar peduncle, scale bars in (A-E), 1 mm; scale bars in (A'-E'), 200 μm. Representative images from a replicate of one mice are shown.

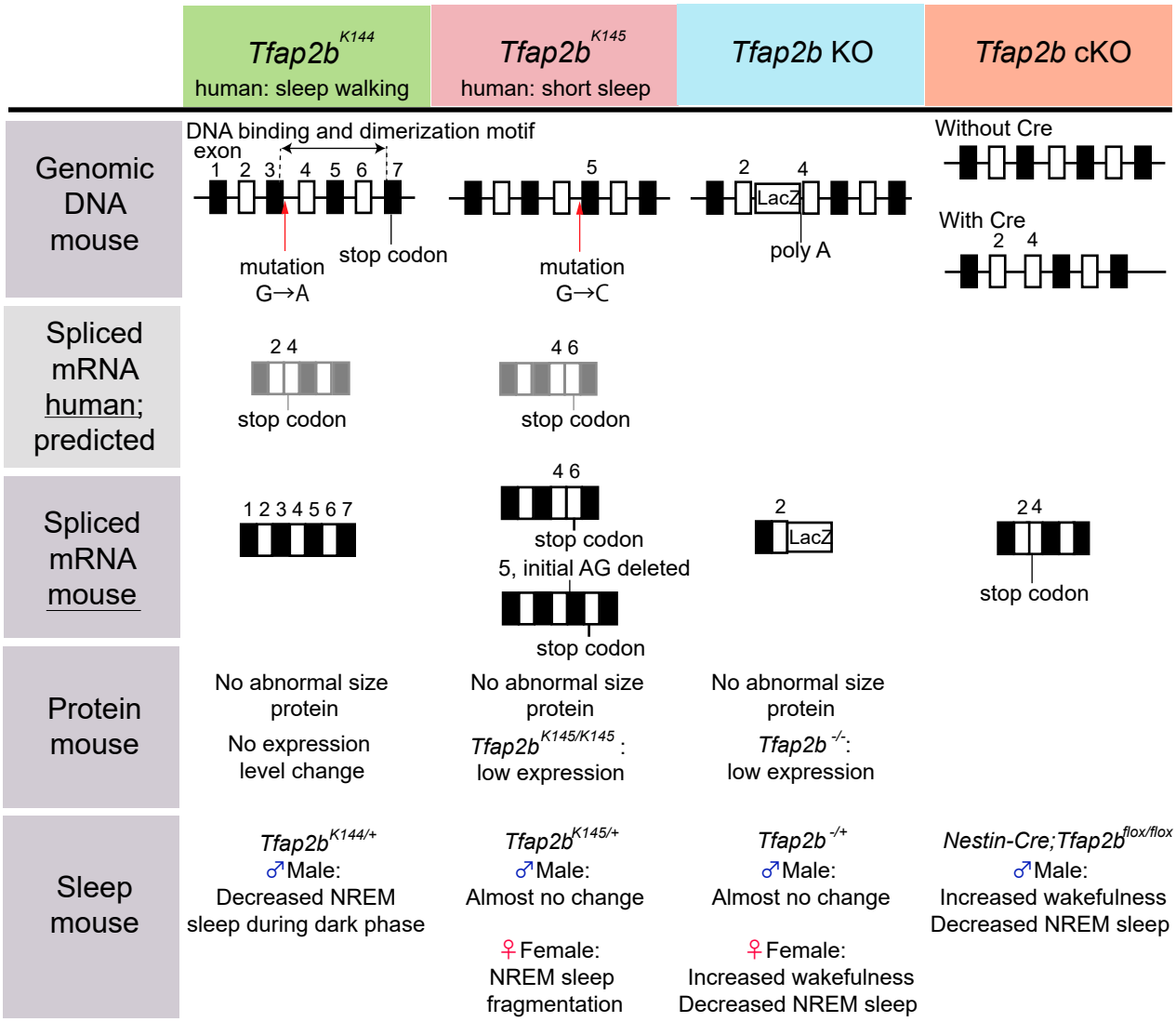

Fig. 21. Summary of the information on gene mutation and mRNA, protein, and sleep phenotype